2004

Seismic and gravity investigation of sediment depth bedrock topography and faulting in the Tertiary Flint Creek basin western Montana

Jeremy C. Stalker
The University of Montana

SEISMIC AND GRAVITY INVESTIGATION OF SEDIMENT DEPTH, BEDROCK TOPOGRAPHY, AND FAULTING IN THE TERTIARY FLINT CREEK BASIN, WESTERN MONTANA

By

Jeremy C. Stalker

B.S. in Geology from Michigan State University

A Thesis submitted in partial fulfillment

of the requirements for the degree

MASTER OF SCIENCE

In

Geology

The University of Montana

Chairperson

Dean of Graduate Studies

5-24-04

Date

Stalker, Jeremy C. M.S. May 2004 Geological Sciences

Seismic and Gravity investigation of the Bedrock, Sediment depth and Faulting in the Flint Creek Basin, Drummond, MT.

Director: Dr. Steven Sheriff

The Flint Creek basin is a NE-SW trending intermontane basin within Montana's fold and thrust belt. It is located in the extensional system between the Bitterroot and Deer Lodge Valleys, both north-south trending Tertiary half-grabens. The bedrock in the Flint Creek basin consists of Cretaceous aged sedimentary rocks in the eastern portion with Precambrian Belt Supergroup thrust over Paleozoic rocks in the western side. I have been complementing geologic mapping of the area with a mix of seismic and gravity observations to better determine the geometry of the Tertiary faulting and sedimentation during the basin's growth. The complete Bouguer gravity data includes 598 existing stations and 50 new observations spaced roughly 300 meters apart. The wide spacing maximizes coverage of the whole basin while sacrificing resolution of smaller fluctuations in bedrock depth. The resultant gravity model is consistent with the classic extensional structural style in the flanking Deer Lodge and Bitterroot valleys. Seismic data include 6 refraction lines in three separate areas for about 1 km of new reversed seismic refraction data. These data as well as bedrock well analysis reinforce the gravity model of depth to bedrock. Gravity cross sections show sediment depths from 10-1000m and normal faults with initial displacement estimations of up to 600m. The refraction data shows bedrock depth from 10-100 meters and normal faults with displacements of up to 60 meters. In the Coberly-Gulch section, the seismic identification of a normal fault provides a new explanation for observed changes in surficial geology. Those data also constrain the age of the end of basin-bounding faulting to the middle Miocene

Acknowledgements

I would like to thank my Advisor Dr. Steve Sheriff for his guidance, teaching and overall, his patience, Dr. Marc Hendrix for the idea to work in the Flint Creek Basin and basin analysis skills, and Dr. Donald Potts for his help as a reviewing committee member. In addition I need to thank my field volunteers, Nate Harrison, Amy Bondurant, Sheetal Petal, Eric Katvala, Christina Mosolf, Kate Glaccum, and Moby for all their help, I could not have done this without them. I also need to thank the USGS Educational Cooperative mapping program and the McDonough Scholarship donors for financial support, and finally my mother Jackie, and my Father James for support and helping me believe I could continue to do what I love.

Table of Contents

List of Figures

List of Tables

Introduction

The Flint Creek basin is a small intermontane basin approximately 5km wide and 10km long (Fig 1). It is bounded on the western and southern edges by the John Long Mountains, on the eastern edge by the Flint Creek Mountains, and on the northern boundary by the Garnet Mountains and the Lewis and Clark Fault system. The basin strikes NE-SW, is widest in the north, and tapers to the south. Tertiary basin fill is the primary aquifer in the valley but high water-producing lenses are thin and discontinuous. With the population in the western Montana intermontane basins growing at a rapid rate better understanding of the basin's geometry and its sedimentary fill is needed to meet the demands of water use and regulation.

This purpose of this study is to use a geophysical approach to determine the bedrock geometry of the Flint creek basin. Similar studies have been conducted in the flanking Bitterroot, Missoula and Deerlodge basins (McLeod, 1987, Evans, 1997, Wells, 1984). Typically, a modestly spaced gravity survey yields an excellent first guess at the shape of bedrock and basin fill in such valleys (Wells, 1984, Hall et al., 1962, Wolfe et al., 1996, Ibrahim, 1972, Healy et al., 1964, Evans, 1997, Nyquest, 2001). 598 gravity observations for the area are available from the National Geophysical Data Center. I added 50 new gravity observations to the existing data to help estimate the Flint Creek Basin's sediment depth and geometry. Points of known bedrock depth in the basin would increase the accuracy of any depth model. Since there were few reliable sources of bedrock data, I conducted six seismic refraction surveys to locate depth to bedrock and help constrain the gravity model.

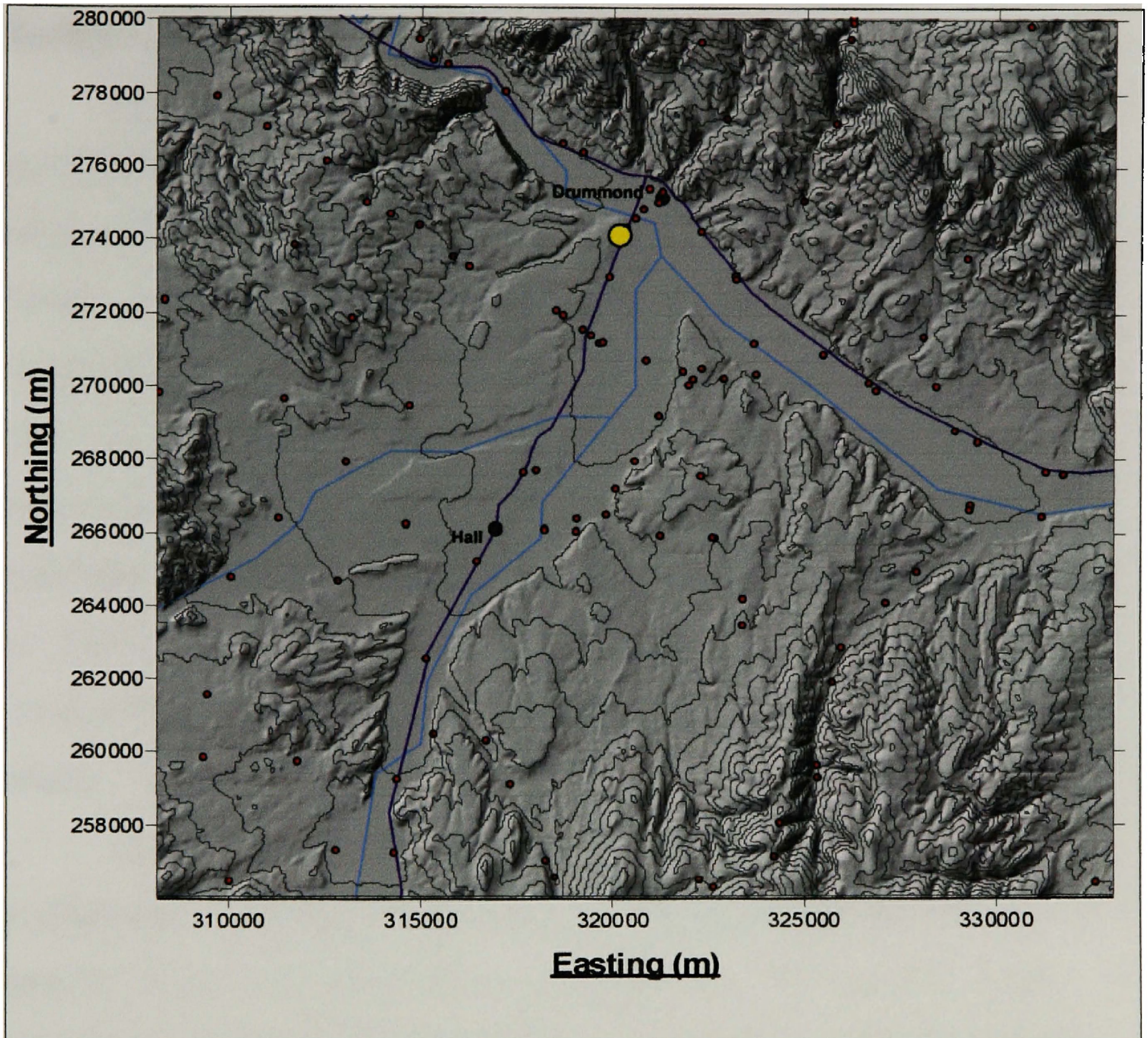

Figure 1. Shaded relief map of the Flint Creek Basin. Blue lines are rivers and creeks. Purple lines are highways, and red points are gravity stations. Gravity and GPS base station in yellow. Northing and Easting in Montana State Plane

Geologic Setting and Previous Work

The Flint Creek Basin shares a similar geographic appearance and geologic history with other larger basins in Western Montana. The Bitterroot, Jefferson, Grasshopper, and Deerlodge valleys all strike north to south, contain Tertiary basin fill, are bounded by normal faults, and are modeled as grabens or half grabens (Fields et al., 1985, Rasmussen, 1969, Rasmussen, 1973, Axelrod, 1984, Axlerod, 1987, Matoush, 2002, Wells, 1984). Following widespread crustal shortening from the Late Jurassic to Cretaceous, the thickened crust began extending through the Tertiary as part of the Basin and Range province (Fields et al., 1985, Janecke, 1994). A series of extensional basins, filled with Tertiary conglomerates, sands, silts, and volcanic ash, developed between mountain ranges.

Major normal fault movement in the Deerlodge, Grasshopper, and Missoula basins occurred in the Eocene with smaller movements in the mid-Miocene (Fields et al., 1985, McLeod 1987, Matoush, 2002, Janecke, 1994). The Renova Formation (Oligocene) or its age equivalent, as well as the Sixmile Creek Formation (Late Miocene-Early Pliocene), fills most of these basins with volcanic input from large volcanic eruptions originating from the Cascade range and Yellowstone, and smaller inputs from local volcanic sources. An angular unconformity between the Renova and Sixmile Creek formations crops out in the Flint Creek and Missoula basins and can be seen in boreholes in the Deerlodge

Valley (Rasmussen, 1973, Portner, 2004, McLeod, 1987) suggesting active faulting, or severe erosion between the Renova and the deposition of the Sixmile Creek.

The John Long Mountains of the western boundary and the bedrock of the southern boundary are composed of Precambrian Belt Supergroup, as well as scattered Mesozoic rocks (Fig. 2). Cretaceous rocks of the Kootenai formation and the Colorado group make up the bulk of the bedrock on the eastern margin of the basin with smaller outcrops of the Permian Phosphoria, and Jurassic Swift, Reirdon, and Sawtooth formations (Bhatt, 1967, Fields et al., 1985, Portner, 2004, Lewis, 1998) further south. These rocks also include mafic Tertiary intrusions (Kunz, 2003), which are important for my density considerations. The Lewis and Clark fault zone is the northern structural boundary of the basin and may contribute to the magnitude of subsidence in the Flint Creek basin (Sears et al., 2000). The distribution and characteristics of rocks at the surface are fairly well known. The surface geology provides constraints on models of the subsurface and density estimates.

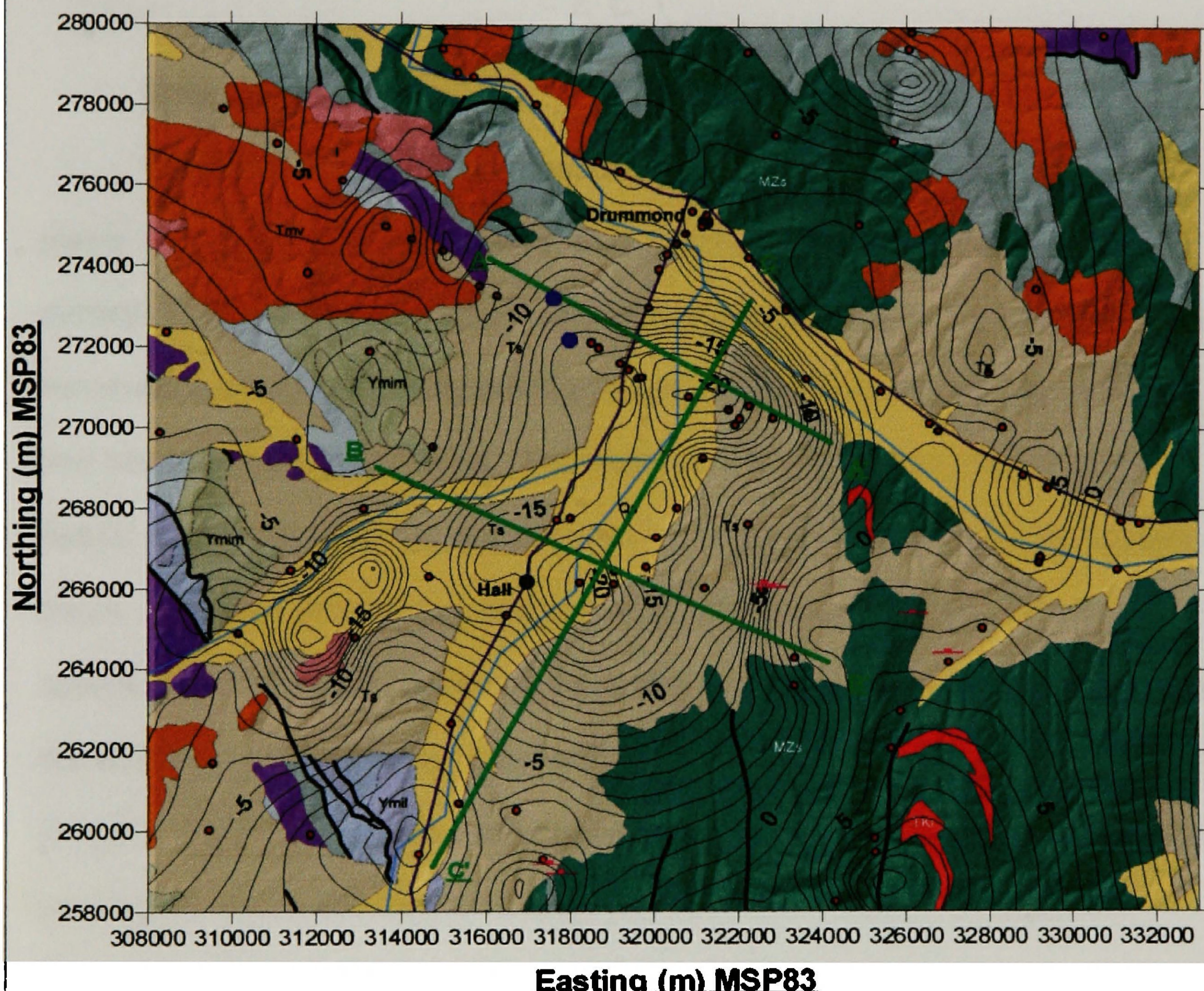

Fig 2: General geologic map of the Flint Creek basin. Contours are residual gravity. Red dots are gravity stations. Green lines are 2D cross sections. Black lines are faults. Pink lines are seismic refraction lines, and blue circles represent wells, which penetrate to bedrock. (Lewis, 1998 1:250k Butte Quadrangle)

Methods

Seismic Refraction

Accurate bedrock depth measurements, such as wells, are scarce and poorly distributed in my study area, thus I conducted six seismic refraction surveys to establish some initial estimates of bedrock depth, which I then used to constrain subsequent gravity models augmenting observed geologic structural and stratigraphic observations. The location of the refraction lines (Fig 2) was based on geologic interest, access, and detection limits of the seismic system. I chose two areas of relatively well known subsurface stratigraphy to determine seismic velocity, which could later be applied in areas where we are less sure of the subsurface stratigraphy. The first area is 1.5 km up Douglas Creek road. The Douglas Creek line samples an area where Tertiary is deposited uncomformably over tightly folded and faulted Cretaceous bedrock, which in turn lies unconformably over Precambrian rocks. The second area was on the flank and on the crest of Dunkelberg ridge, which is mapped as Tertiary over Cretaceous on the flank, and Cretaceous on the crest of the ridge. The final line was taken on unknown stratigraphy in the Coberly Gulch area.

In total, I collected about one kilometer of reversed seismic refraction data using a Geometric 24-channel Smartseis seismograph (Fig 3). For each seismic experiment, twenty-four 14Hz geophones were spaced 5m apart. The geophones were buried in 6-12 cm of soil to maximize contact and minimize noise. The seismic source, a Bison-1 elastic wave generator (Fig 4), was placed at 10m, 20m, 40m or 60m from the end of the survey lines for all experiments. Typically, in the field, I could resolve clear first breaks from geophones up to 180 meters from the source.

Figure 3. Author operating the Geometric Smartseis 24 channel seismograph. Geophones (orange) and wave generator are in the background.

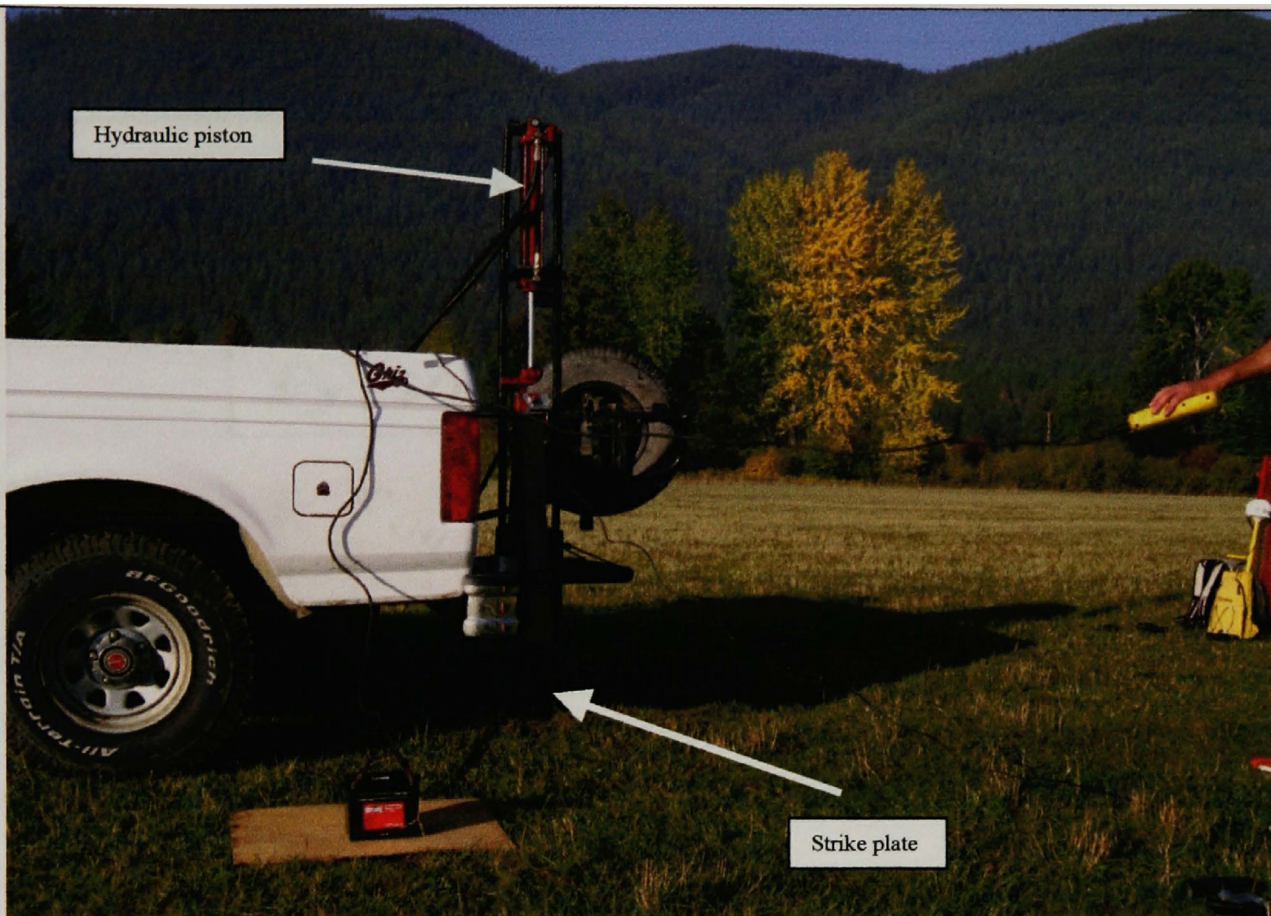

Figure 4. Bison I Elastic wave generator. Note tail hitch mount and hydraulic hand operation. Strike plate is directly beneath the red piston. The inertial switch to the seismograph is attached to the strike plate

Seismic Analysis and Results

I analyzed the seismic data using SIPWIN (Rimrock Geophysics, 1999), a commercial program that inverts results from refraction experiments for subsurface depth and velocity sections. I analyzed the wave traces resulting from a survey to pick the first arrival of the refracted waves to each geophone (Fig 5). This process can be somewhat subjective, especially if the returns are noisy. The program does allow the user to turn off noisy phones and calculate velocities using only the clear phones. The program then calculates velocities using an iterative ray path tracing technique and forward modeling of layer thickness. Depth and velocity error can result from the choice of layer assignments, but reasonable interpretation of wave traces from user to user should result in very similar velocity cross-sections.

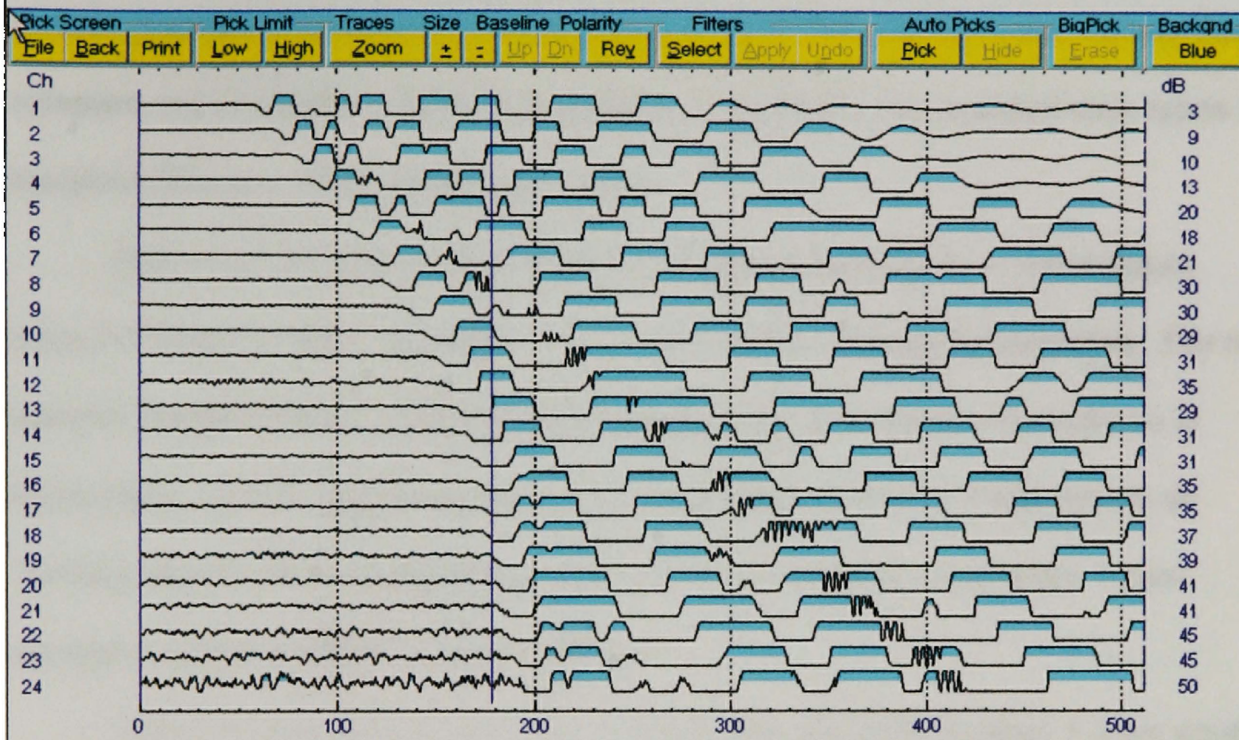

Figure 5. Sample refraction trace display. Vertical axis on left is geophone number; on right is the decibel gain of the phone. Horizontal axis is time in ms.

I evaluated the stratigraphy in each of the cross sections SipWin produced by comparing published velocities of similar lithologies and using mapped surface geology and structural relationships. I will first discuss each survey then compare my observed velocities to those published for the mapped rock types in literature (Burger, 1992, Ryenolds, 2001).

Note that the Sixmile and Renova formation sediments in most cases have indistinguishable velocities due to very similar lithological densities. For my seismic interpretations, differentiation between the two Tertiary formations is speculative, and in the remainder of this document, I refer to these layers as Tertiary unless other stratigraphic information is available. (Appendix 1 has complete seismic refraction information.)

Seismic lines 9-21-1 and 9-21-2 (Fig 6 a/b) are both located 1.5 km south east on Douglas Creek road on Cominco Mining Corp. property (Fig 2). The geology in this area was previously mapped (Lewis, 1998, Portner, 2004, Gwinn, 1960) providing me with good control on the stratigraphy.

The geology below line 9-21-2 (Fig 6b) is better understood, and velocities from this line are used as velocity controls for similar lithologies in other areas. This survey was also located directly on rocks mapped as Tertiary Sixmile Formation and yields a 500 m/s velocity estimate. The next deeper velocity layer is the more competent, (1100m/s) and probably representative of the Tertiary Renova formation. The Tertiary in this section is 60m thick with a small undulation possible caused by faulting in the bedrock under geophones 3, 4 and

5 (Fig. 6b). The 3500 m/s layer represents Precambrian bedrock, or Triassic Quadrant formation.

Line 9-21-1(Fig 6a) is closer to the mouth of Douglas Creek about half a kilometer northwest of line 9-21-2. The layer nearest to the surface has a velocity of 510 m/s, which reflects the unconsolidated Tertiary of probable Sixmile composition. The next 1800 m/s velocity layer is consistent with published values for shale, and probably represents shale from Cretaceous sediments. The last detectable velocity of 3043 m/s could be limestone of the Cretaceous Kootenai or Colorado group, Precambrian belt quartzite and argillite, or the Quartzite of the Triassic Quadrant formation. Due to complex faulting and similar lithologies, differentiation between the Cretaceous, Triassic, and Precambrian formations was not possible. The Tertiary section on this line either way is 50m thick with the bedrock surface appearing fairly uniform for the length of the survey.

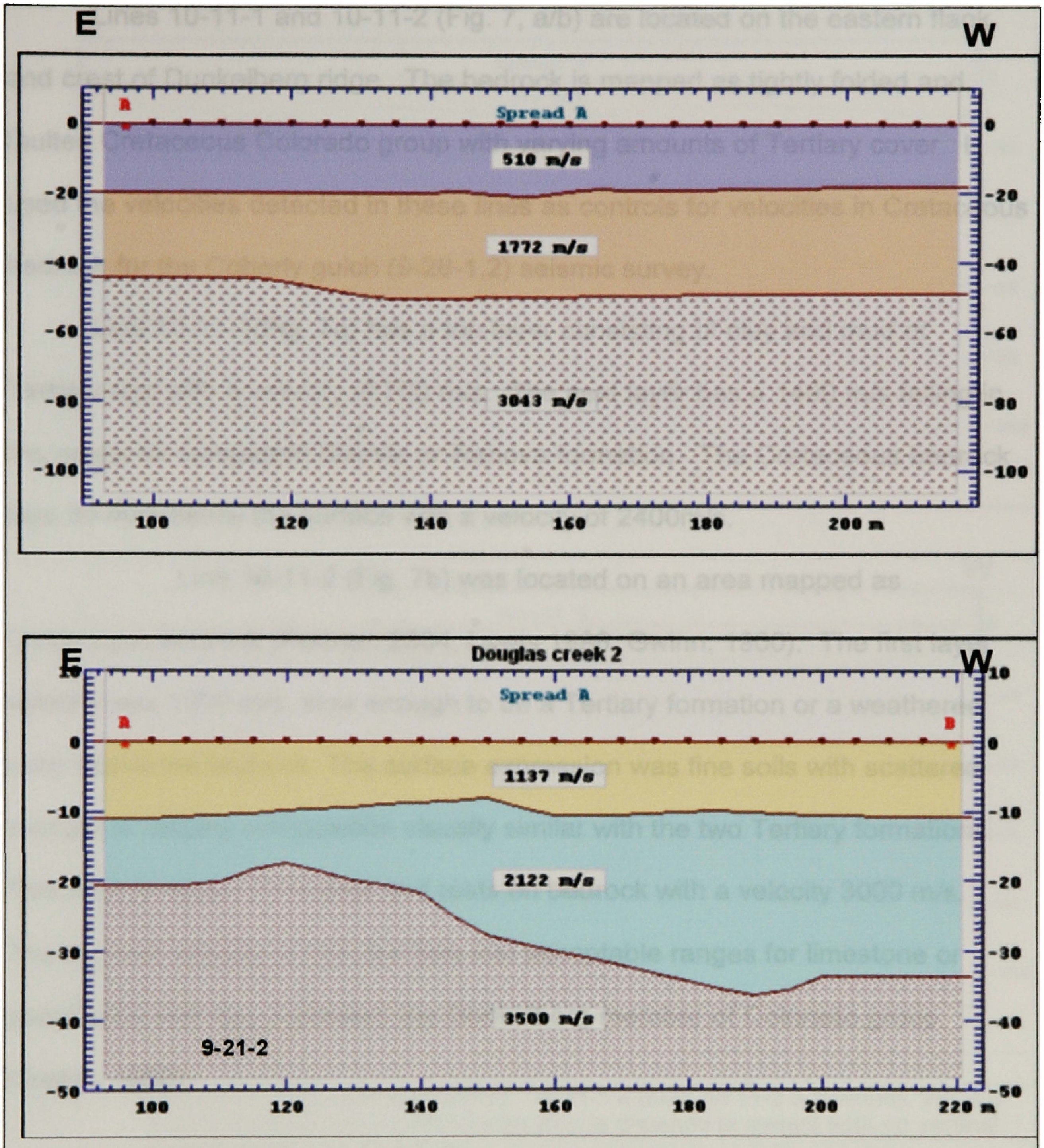

Figure 6. Douglas creek seismic profiles. 9-21-1 a (top). 9-21-2 b (bottom). Vertical axis is depth in meters. Horizontal is distance in meters. Vertical exaggeration is 1:2

Lines 10-11-1 and 10-11-2 (Fig. 7, a/b) are located on the eastern flank, and crest of Dunkelberg ridge. The bedrock is mapped as tightly folded and faulted Cretaceous Colorado group with varying amounts of Tertiary cover. I used the velocities detected in these lines as controls for velocities in Cretaceous bedrock for the Coberly gulch (9-28-1,2) seismic survey.

Line 10-11-1(Fig. 7a) has a top layer consisting of clay and mud of Tertiary age with a velocity of 700 m/s. The next layer has a 1400 m/s falling in the range for competent Sixmile or Renova formation. The Cretaceous bedrock lays 30-40m below the surface with a velocity of 2400m/s.

Line 10-11-2 (Fig. 7b) was located on an area mapped as Cretaceous bedrock (Portner, 2004, Lewis 1998, Gwinn, 1960). The first layer velocity was 1300 m/s, slow enough to be a Tertiary formation or a weathered zone above the bedrock. The surface expression was fine soils with scattered cobbles of varying composition visually similar with the two Tertiary formations. This layer is about 10 m thick and rests on bedrock with a velocity 3000 m/s. The bedrock velocity is high but falls into acceptable ranges for limestone or porcelanite and may represent the Dunkelberg member of Colorado group (Gwinn, 1960).

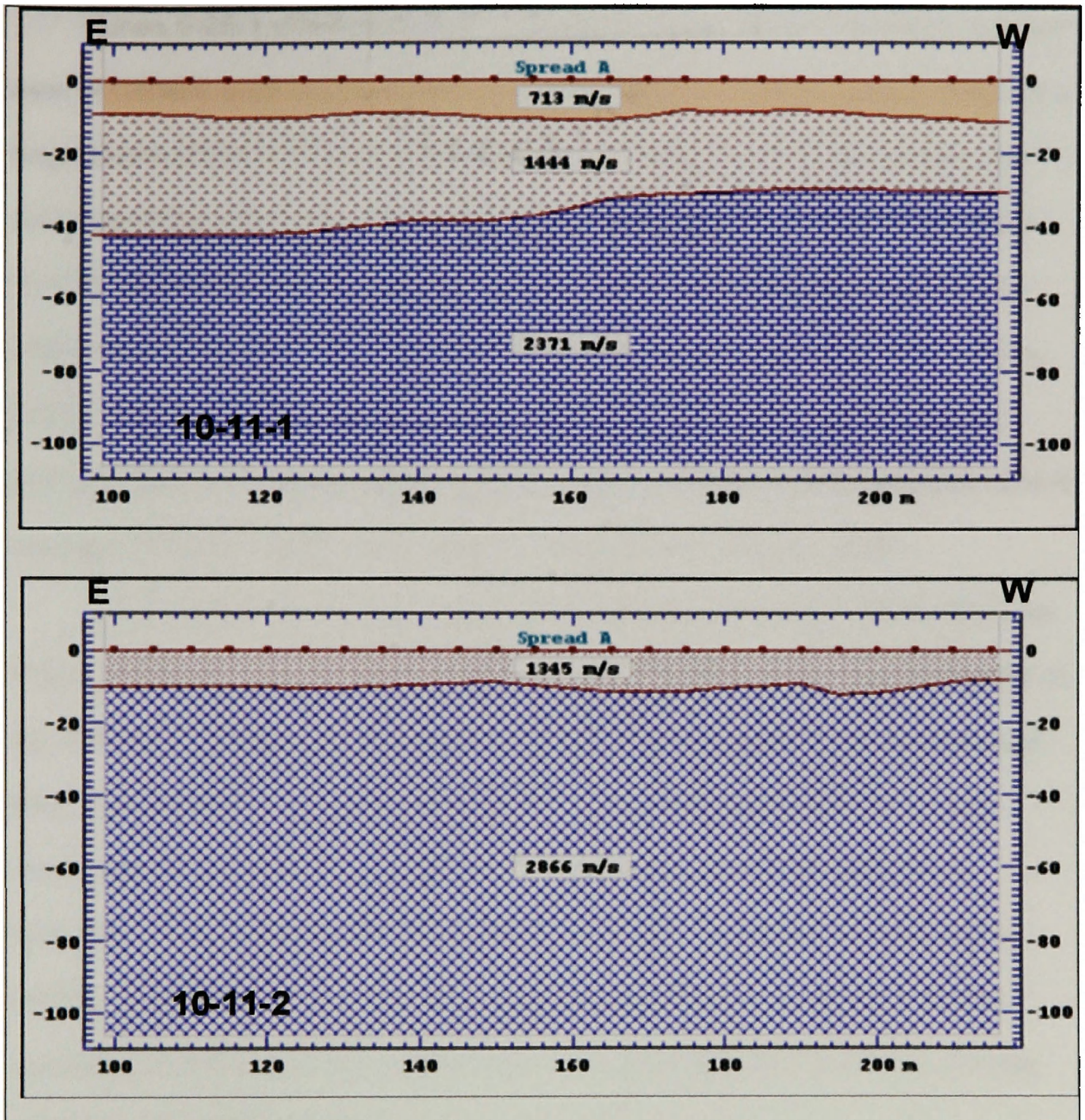

Figure 7. Dunkelberg ridge seismic profiles. 10-11-1 a (top), 10-11-2 b (bottom). Vertical axis is depth in meters. Horizontal axis is distance in meters with no vertical exaggeration

Lines 9-28-1 and 9-28-2 (Fig. 8 a/b) are located up Barnes Creek road just west of Coberly gulch on Dingwall Inc. ranch property. These surveys detected a large displacement in the subsurface visible in Fig 8a. Due to the western dip and drop of the head wall to the west, I believe this is a normal fault with about 60 m of displacement that appears to affect both Colorado group and Renova sediments within this survey line. This fault would help explain why the Tertiary section exposed east of Coberly Gulch seems thin compared with equivalent beds exposed further west. Additionally a similar fault with similar displacement is exposed half a kilometer to the west in Barnes Creek (Portner, 2004)

Line 9-28-1(Fig. 8a) was collected on Tertiary sediments I assumed to be of Sixmile Creek age due to size and composition of the large cobbles present on the surface. The upper layer velocity of 500 m/s is consistent with the previous seismic observations of Sixmile formation. The next layer of 800 m/s, I also interpreted as Tertiary. The Tertiary sediments in this line total 30-60 m in thickness. The Cretaceous bedrock layer is 30-60m below the surface with a velocity of 2200 m/s. This velocity is high compared to the competent Tertiary velocities observed in other seismic lines, and is most likely sandstone or shale of the Cretaceous formations.

Line 9-28-2 (Fig 8b) was directly in line with 9-28-1; thus, the two constitute a continuous seismic profile. Line 9-28-2 displays a similar velocity cross-section to that of Figure 8a, but a deeper bedrock depth of 30-70m. This line contains the large offset seen under geophones 13-22. I interpret this feature is a normal fault, with a displacement of at least 40m, dipping west at an

80° angle. The fault displaces both Cretaceous and early Tertiary aged rocks and drops the bedrock depth from 30m on the footwall to 70m on the headwall. I cannot determine if it displaces the Sixmile formation, it does however appear the Sixmile formation sediments are thinner on top of the footwall of the fault. This fact would help constrain the earliest movement of the fault during the Early Eocene emplacement of the Sixmile Creek formation.

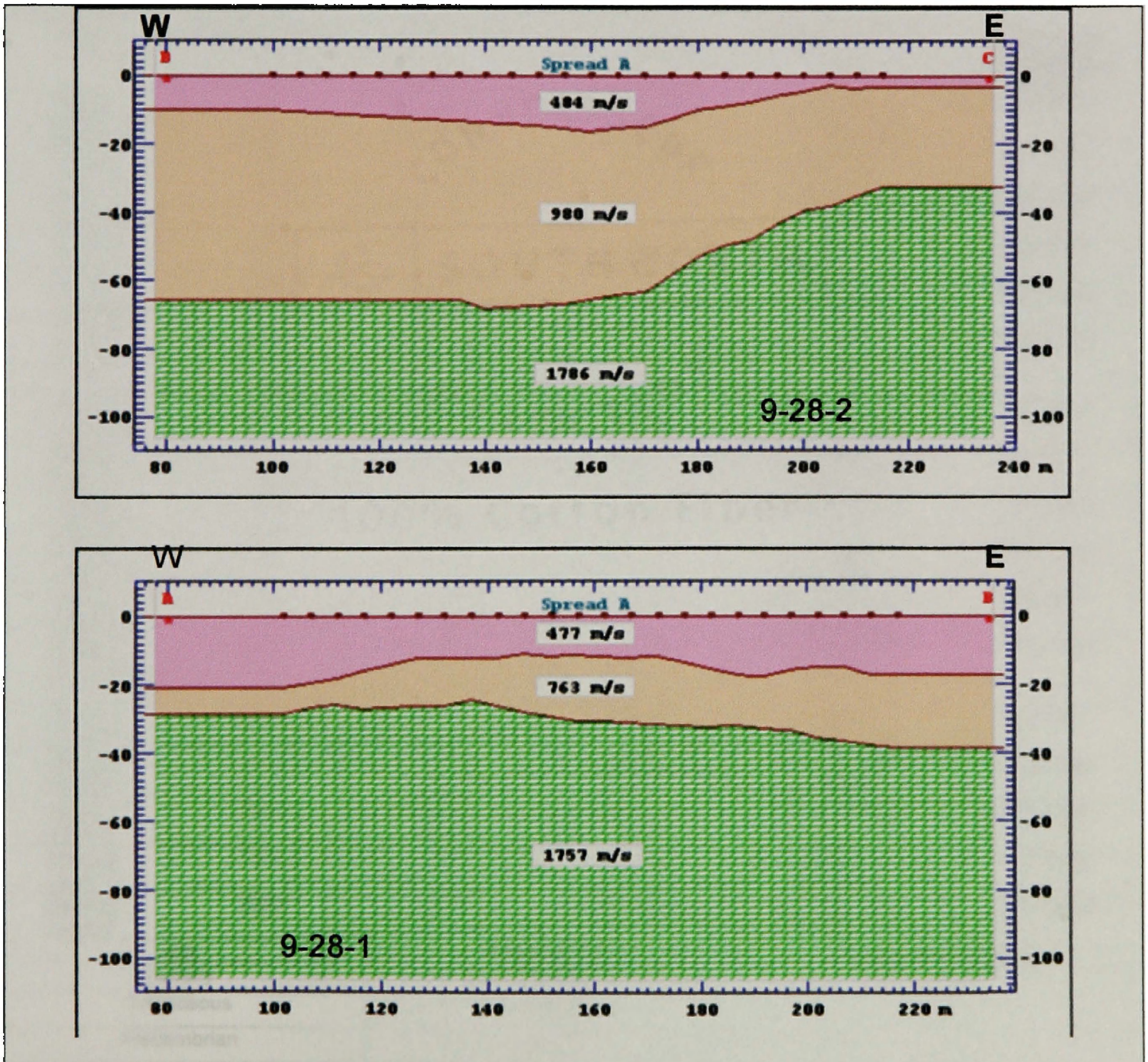

Figure. 8: Coberly gulch seismic profiles. 9-28-1 a (top), 9-28-2 (bottom). Note large displacement in top right this is interpreted as a small normal fault. Vertical axis is depth in meters. Horizontal is distance in meters.

A summary of the layer velocities and their comparisons to published values is presented on Table 1. The highest amount of variance occurred in the Cretaceous, this is probably due to the heterogeneity, and extreme folding and faulting in the section. I only encountered one Precambrian velocity, thus I could not compare it with other observed velocities, instead I compared it to published values for Precambrian quartzite in Montana (Burger,1994)

Line #	Velocity (m/s)	Thickness (m)	Interpreted Lithology (Age)	Formation and rock type	Theoretical Velocity Range (m/s)
9-21-1 Layer 1	510	19	Tertiary	Sixmile Conglomerate	400-2300
9-21-1 Layer 2	1800	31	Cretaceous	Colorado Grp Sh/Ss	1400-4500
9-21-1 Layer 3	3000	60+	Cretaceous	Kootenai? Lms	2700-3600
9-21-2 Layer 1	1200	20	Tertiary	Renova? Mudstone	300-1800
9-21-2 Layer 2	2200	45	Cretaceous	Kootenai Ss/Lms	1400-4200
9-21-2 Layer 3	3500	45+	Precambrian	Belt Qrtzite?	3300-5000
9-28-1 Layer 1	480	10-20	Tertiary	Sixmile Conglomerate	400-2300
9-28-1 Layer 2	770	10-20	Tertiary	Sixmile/Renova? Mud/Sand	300-1800
9-28-1 Layer 3	1800	70+	Cretaceous	Colorado Grp. Ss/Sh	1400-4500
9-28-2 Layer 1	500	4-10	Tertiary	Sixmile Conglomerate	400-2300
9-28-2 Layer 2	980	20-55	Tertiary	Sixmile/Renova? Mudstone	300-1800
9-28-2 Layer 3	1800	50-80+	Cretaceous	Colorado Grp. Ss/Sh	1400-4500
10-11-1 Layer 1	700	10	Tertiary	Sixmile Conglomerate	400-2300
10-11-1 Layer 2	1500	20-30	Cretaceous	Colorado Grp Ss/Sh	1400-4500
10-11-1 Layer 3	2400	70-80+	Cretaceous	Colorado Grp. Lms	2700-3600
10-11-2 Layer 1	1400	10	Cretaceous	Colorado Grp. Ss/Sh	1400-4500
10-11-2 Layer 2	2900	100+	Cretaceous	Colorado Grp. Lms	2700-3600

Age	Mean velocity	Standard deviation
Tertiary	605	182
Cretaceous	2000	570
Precambrian	3500	0*

Table 1. Velocity comparisons for seismic lines average velocity for each age sediment and standard deviation. *Only one Precambrian observation was available. This value was compared with values published in literature (Burger, 1994)

The seismic lines provide me with control points of well constrained depth to bedrock in the eastern portions of my basin, which will directly help me constrain my 2D and 3D sediment depth models. The orientation and location of a normal fault, and layer thickness provide data on statigraphic relationships, Tertiary depth and composition, fault location, and bedrock topography, all help with the collaborative mapping efforts of Portner (2004) and future studies on basin evolution and fault timing.

Gravity and GPS

I conducted a gravity survey of the basin to determine the shape of the bedrock beneath the basin as well as to help constrain models of the distribution of sediment depth within the basin. Obviously the distribution and orientation of rocks at the surface provide constraints for the final solutions as do two existing wells which bottom in bedrock, and the seismic data presented above. To augment 598 existing data points from the National Defense mapping Program, I collected 50 new gravity measurements with accompanying GPS coordinates and elevation. (Appendix 2 has GPS station information; Appendix 3 has gravity stations and corrections)

Accurate elevation control is critical to accurate gravity measurements. Therefore, I measured latitude, longitude, and elevations using a Trimble XRS PRO GPS system (Fig 9). I acquired the location data in carrier phase mode, gathering 6-10 minutes of signal at each station. These data were later post-processed using differential corrections from a stationary GPS unit and a real time correction broadcast from the Flathead Lake Coast Guard station in Polson, MT. Previous work in the area using similar procedures with this equipment yielded elevations with standard deviations of about 0.3 m (Evans, 1997, Nyquest, 2001). I made multiple measurements at my GPS base station just over the Route 1, Clark Fork bridge near Drummond, MT (Fig 1). I reoccupied the GPS base station at the beginning and end of each field day, which yielded twelve repeat measurements over a 5-month period (Table 2).

Figure 9. Author operating the Trimble XRS PRO GPS system

Date	Measurement Name	Easting (m)	Northing (m)	Elevation (m)
2/22/2004	1C	320300.98	274319.67	1215.83
2/22/2004	10C	320300.98	274319.67	1215.83
11/15/2003	1A	320299.75	274318.43	1215.54
11/15/2003	9A	320299.56	274318.88	1215.43
11/22/2003	1B	320299.38	274318.39	1215.31
11/22/2003	9B	320299.07	274318.14	1215.54
3/1/2004	1D	320299.07	274318.14	1215.54
3/1/2004	7D	320301.08	274319.32	1216.08
3/8/2004	1E	320301.01	274319.64	1215.42
3/8/2004	10E	320301.01	274319.64	1216.02
3/12/2004	1F	320301.01	274319.64	1216.05
3/12/2004	5F	320301.01	274319.64	1215.97
			Average	Stand Dev
		Elevation	1215.7	0.37
		Northing	274319.10	0.63
		Easting	320300.33	0.83

Table 2. GPS base station elevation error. Northing and Easting (meters) are in Montana State Plane 83. Base station is located just over the Clark Fork bridge southwest of the city of Drummond (Fig 1).

GPS measurements have error resulting from ionosphere refraction and systematic error programmed in satellite broadcasts by the Department of Defense. To correct for these errors sources I differentially corrected my field observations using a real time correction broadcast from the United States Coast Guard station in Polson, MT as well as differential correction from a stationary 12-channel Community Base Station GPS recorder at the Missoula County office in Missoula, MT. All of my measurements had real time and differential correction.

Standard deviation for northing, easting, and elevation were 0.63 m, 0.83m, and 0.37 m, respectively after the real time and differential corrections. A +/- 0.37 m change in elevation would change the combined elevation corrections of my measurements by approximately +/- 0.10 mgals. For a mean density contrast of 800 kg/m^3 between bedrock and basin fill, this translates to +/- 5 meters of basin depth.

My gravity measurements were made using a Scintrex CG-3 gravity meter (Fig 10). My goal was to combine the NDMP data with my own observations to construct a uniform grid of gravity observations throughout the basin. Ideal is a tough target; my station spacing varied from 50m-500m depending on private land access and road access. Some areas have sparse station spacing, most notably in the central west and southeast of the study area.

I used the CG3's internal solar and lunar tidal routine to correct gravity measurements for those tidal effects. In addition, I constructed standard drift curves to correct for mechanical linear drift of the instrument. The magnitude of the drift corrections were calculated by reoccupying the base station described above every 3-4 hours. The average instrumental drift was 0.01 mgal/hour.

Figure 10. Author operating a Scintrex S3 gravimeter.

My next step was to apply standard corrections to the gravity data using the equation (Lowrie 1997):

$$CBA = G_{obs} - G_{the} + FAC - SBC + TC$$

Where:

CBA= complete Bouguer anomaly

G_{obs} = observed gravity

G_{the} = theoretical gravity (980,362.158 mgals)

FAC = Free air correction (0.3086 mgal/m)

SBC = Bouguer correction. (-0.11195 mgals/m)

TC = Terrain correction

In order to represent the gravity in the area correctly I needed to establish a point of known gravity at my base station in the Flint Creek Basin (980,362.18 mgals) relative to a point of measured gravity in the region. This analysis provides me with a base line value for G_{obs} to deviate from for each observation. Much like my elevation analysis, I compared 12 measurements at my field base station to 12 measurements made at a point of known gravity located on a concrete bench in the basement of the Science Complex at the University of Montana in Missoula. This point is a Mopo International Gravity Standardization Net 1971 (IGSN71) site (980,432.21 mgals). My field base station gravity value is 980,362.18 mgals calculated from comparison with the Missoula base station.

G_{the} is the theoretical value of gravity considering only for the latitude of the station on the ellipsoidal earth. I calculated it using the following equation (Figure 11., Sheriff, 2004):

Theoretical Gravity (gth)

$$g_{th} = 9.7803267714 * \left\{ \frac{1 + 0.00193185138639 * \sin^2\lambda}{\sqrt{1 - 0.00669437999013 * \sin^2\lambda}} \right\}$$

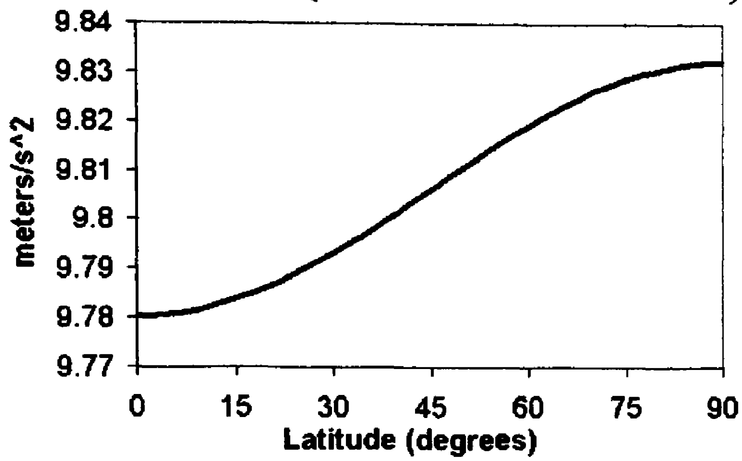

Figure 11. Theoretical gravity correction for the ellipsoidal earth. The closer you get to the north or south poles (90N, 90S) the closer you are to the core of the earth, and thus the higher your value of theoretical gravity. Drummond is at 47 degrees latitude. (Taken from Sheriff,1997)

The free air correction (FAC) accounts for the decreasing gravitational attraction with increasing distance from the center of the earth and is commonly approximated as 0.3086 mgals/m. The simple Bouguer correction was made assuming the distance from the station elevation to the geoid elevation was filled with an infinite slab with a density of 2,670 kg/m^3 yielding a change in gravity of 0.11195 mgals/m. Correction observations by applying G_{the}, FAC, and SBC yields a map of simple Bouguer anomalies.

Transforming simple Bouguer anomalies to complete Bouguer anomalies requires the addition of a terrain correction. My terrain corrections account for the presence of excess mass (mountains) and missing masses (valleys) adjacent to the gravity stations with respect to the infinite slab approximation of the simple Bouguer correction. I used a USGS 30m DEM to produce a composite DEM area of 484 square kilometers with the base station as the center. I divided this composite area into three levels of sample resolution: 30m for the first 5 km X 5 km area, 100m for the next 12 km X 12 km ring, and 250m for the remainder of the area. A terrain correction for each station was calculated using HAMXYZ2 (Gradient Geophysics, 1997). My average terrain correction was 0.59 mgals with a maximum value of 1.12 mgals (Fig 12) near the southeastern portion of my area. The selection of correction area of 22 square kilometers area for the extent of the terrain correction is sufficient for my study as 95% of my stations had a correction of less than one milligal.

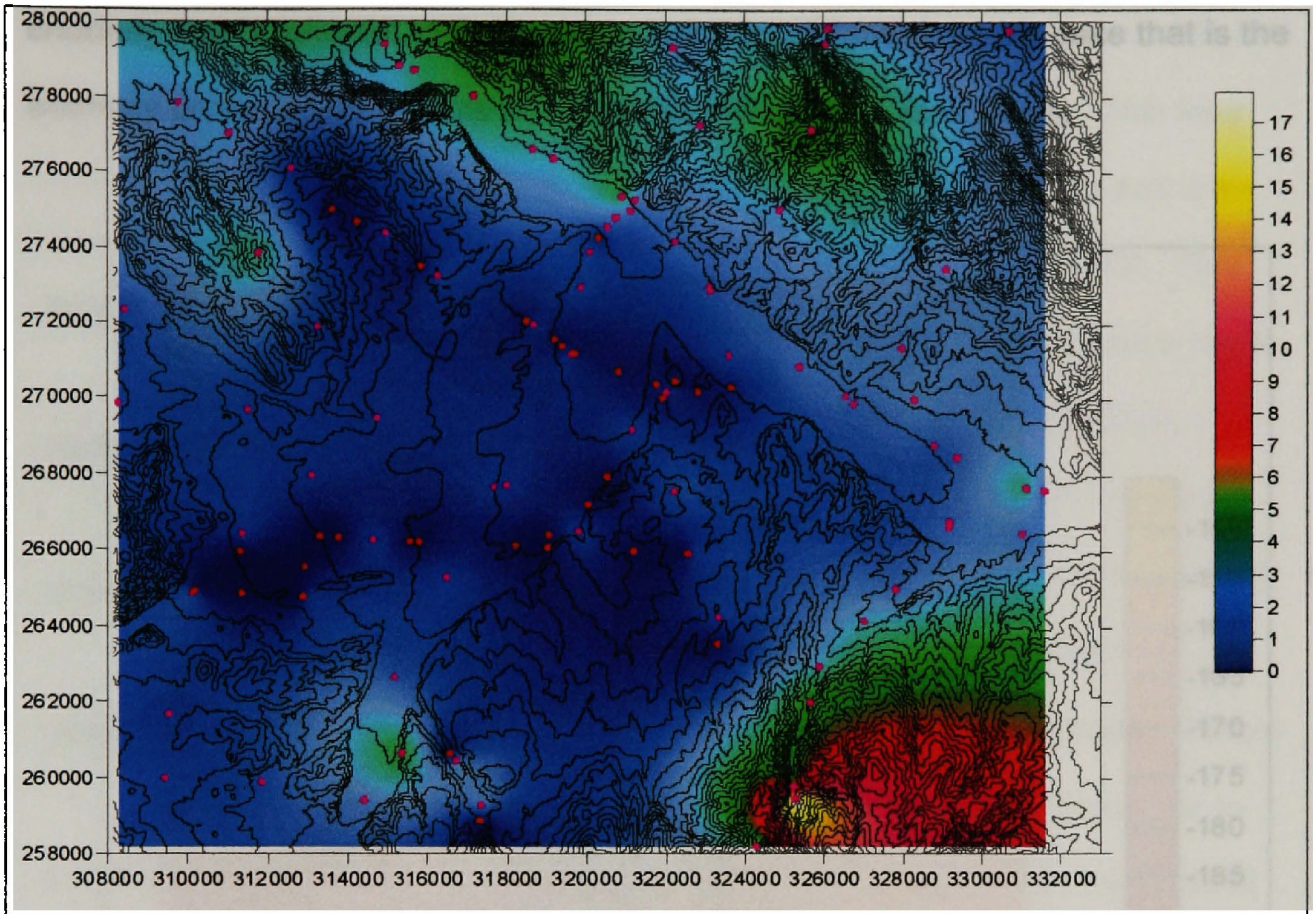

Figure 12. Terrain corrections are in color. The black lines are elevation. Purple points are NDMC data. Red points are my data. Note the majority of my points have a correction less than 1 milligal. Color bar is the terrain correction in milligals. Vertical scale is northing. Horizontal scale is easting. Both are in Montana State plane.

To produce the final map of complete Bouguer anomalies (Fig 13), I combined my new observations with the existing NGDC data. The final distribution of NGDC and my gravity observations (Figs 1, 2) still has some areas of sparse coverage in the southeast of the basin due to access issues.

The complete Bouguer map (Fig 13) shows anomalies caused by both shallow and deep crustal features, as well as the crust/mantle interface. A very important step in any gravity investigation is to isolate the fraction of the total anomaly that is relevant to the problem being investigated. In this case that is the anomaly produced by the shallow features of the Flint Creek Basin.

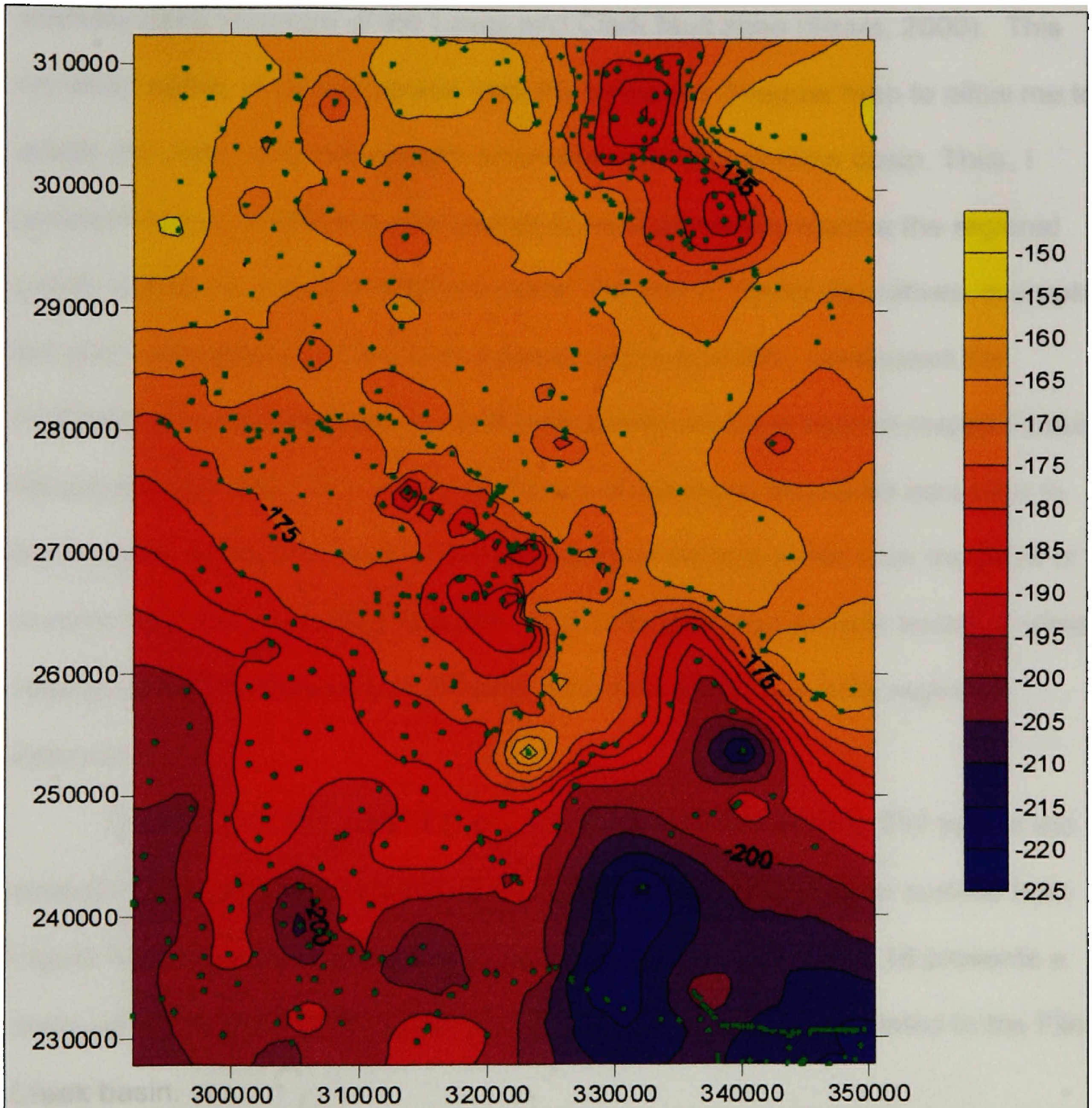

Figure 13. Complete Bouguer Anomaly. Green dots are gravity stations. Vertical axis is northing in meters. Horizontal axis is easting in meters. Scale bar is in Milligals.

The map of complete Bouguer anomalies (Fig 13) has an obvious NE-SW gradient that is of much longer wavelength than the area of interest. This long wavelength feature is related to the deeper crust/mantle relationships and the relatively deep structure of the Lewis and Clark fault zone (Sears, 2000). This signature needs to be subtracted from the complete Bouguer map to allow me to isolate the deep, long wavelength anomalies from the shallow basin. Thus, I compared several different approaches to mathematically resolve the regional gravity signature: a simple digitized plane, 1st and 2nd order derivatives, a simple low pass Gaussian equation, and a power series solution. I evaluated the methods by comparing their residual zero gravity contours against mapped basin fill/bedrock contacts. The gravity signature of the basin should be zero near to the bedrock contact since no mass deficiency or excess exists near the point of change from the basin fill to bedrock. Due to largely inaccessible terrain, I relied heavily on the northeastern and western boundaries for accurate regional determination.

The best solution (Fig 14) was a digitized surface dipping SW across the area of Figure 12 with a slope of -0.61 mgals/km. I subtracted this surface from Figure 12 to produce the residual Bouguer map (Fig 15). Figure 16 presents a close-up of the residual Bouguer anomaly for the area directly related to the Flint Creek basin.

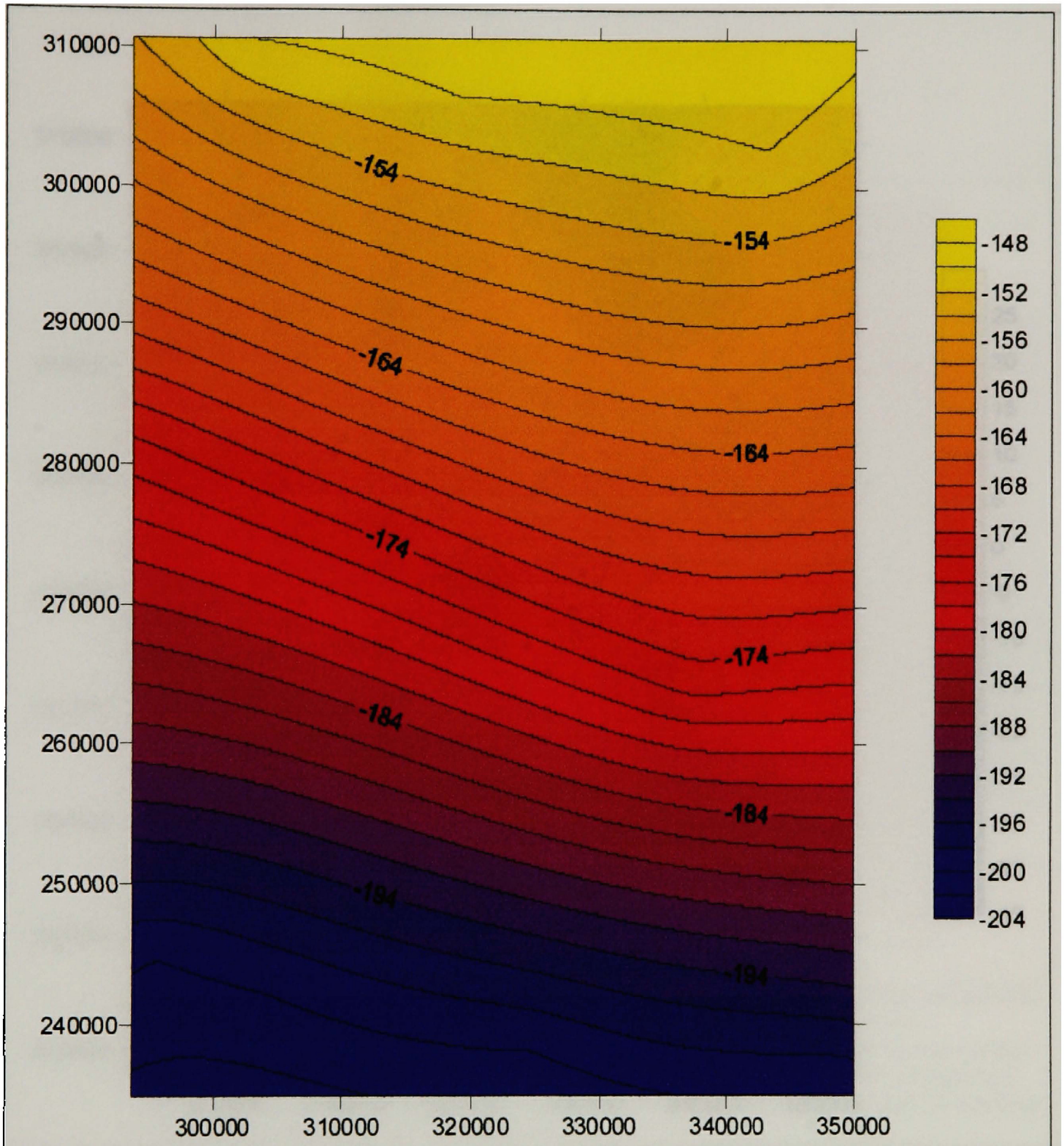

Figure 14. Regional gravity signature caused by deep crust/mantle contacts and regional crustal features. Vertical axis is northing in meters. Horizontal axis is easting in meters. Scale bar is in milligals.

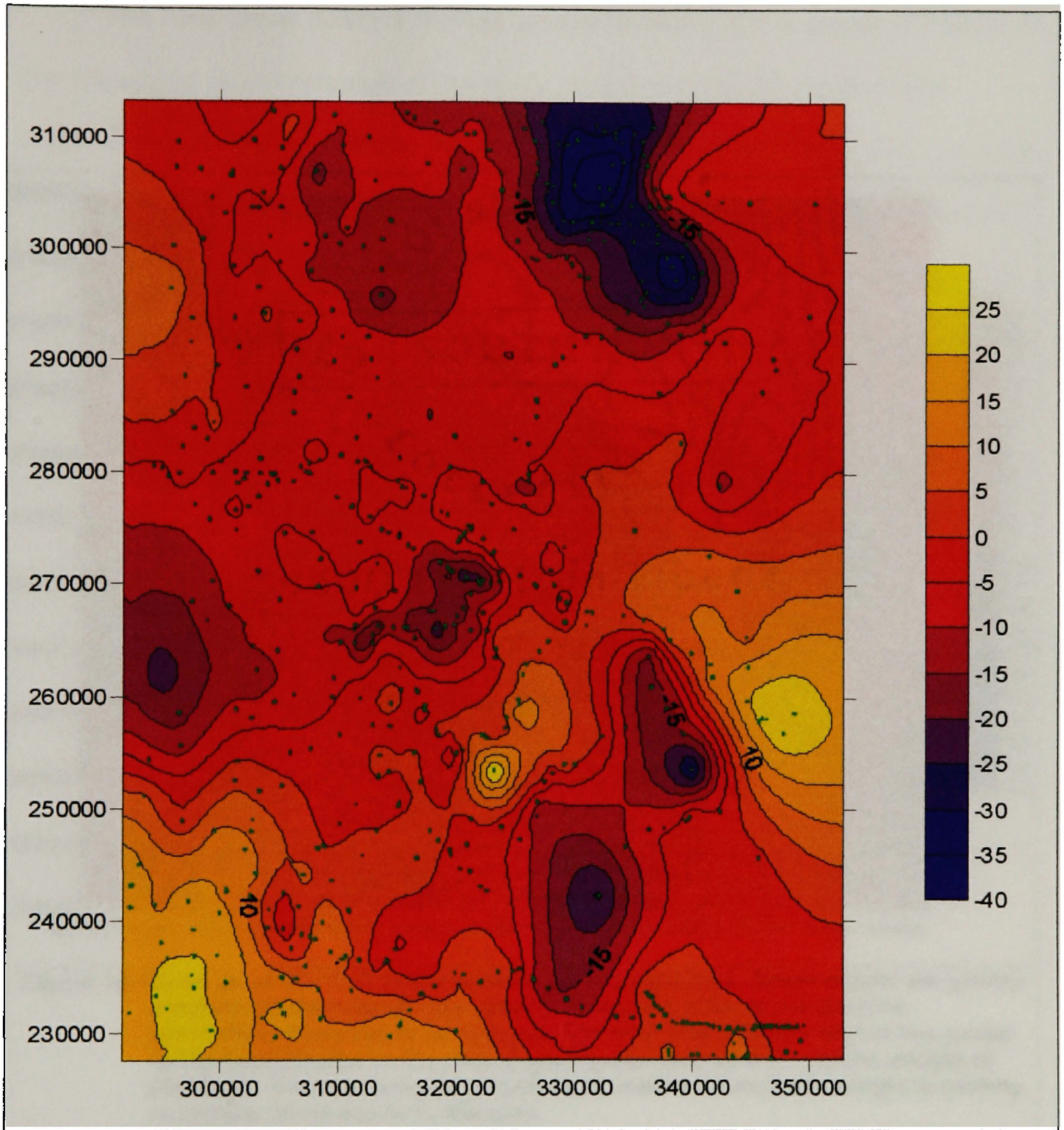

Figure 15. Residual gravity signature (Figure 12 – Figure 13) shows shallow features such as sedimentary basins and shallow intrusive volcanic features. Vertical margin is northing in meters. Horizontal margin is easting in meters. Scale bar is in milligals.

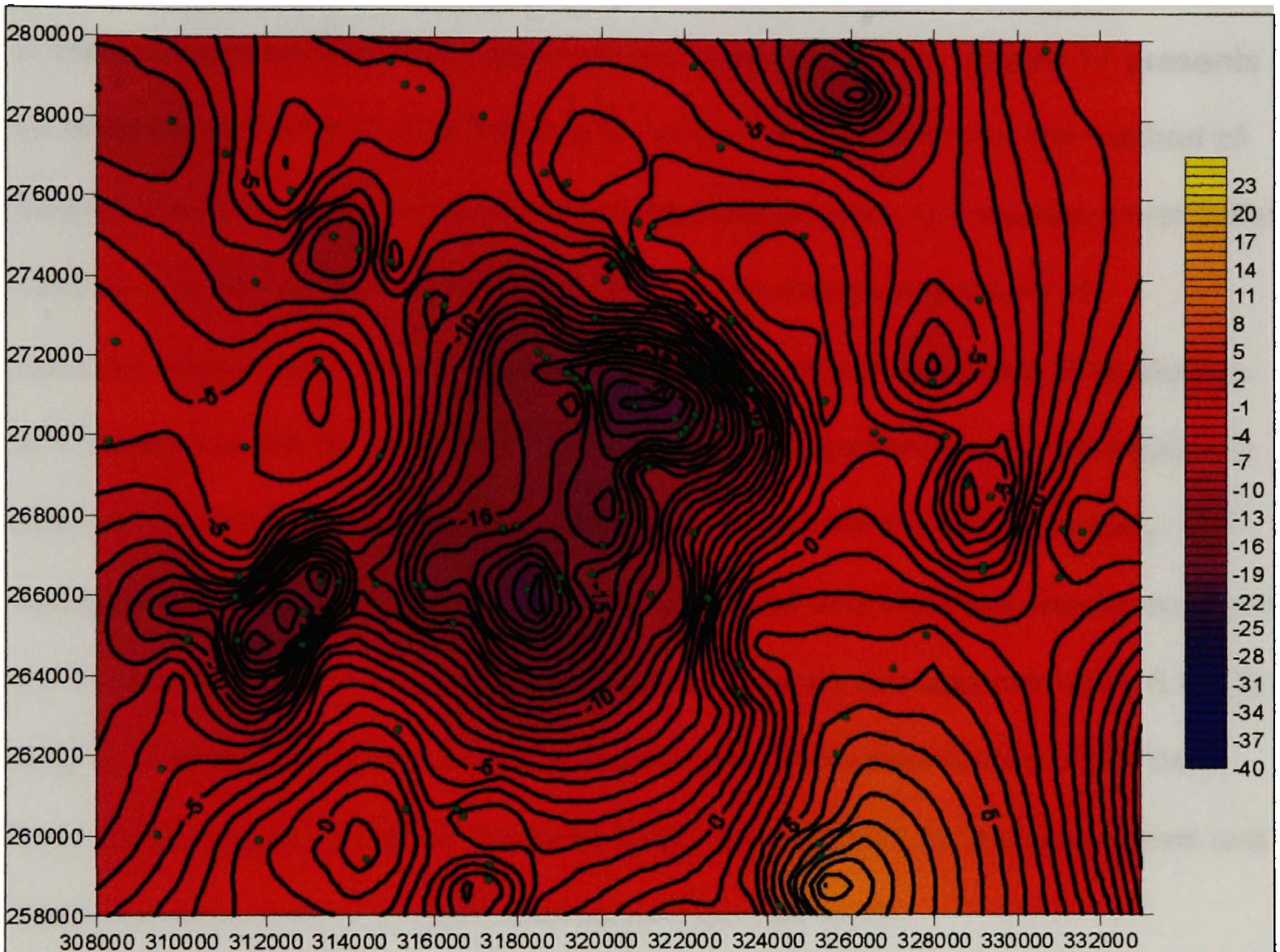

Figure 16. Close up of the Flint Creek basin's gravity signature. Green points are gravity stations; blues indicate low gravity; Reds and yellows are positive anomalies. Scale bar is in milligals. The east west relative high in the center of the basin is due to the lack of gravity stations on the western margin of the basin. Vertical margin is northing in meters. Horizontal margin is easting in meters. Scale bar is in Milligals.

The Flint Creek basin is the low gravity anomaly in the center of Figure 16. The maximum absolute value of the residual anomaly is -20 mgals in the northern section approximately 1km south of the Clark Fork River, and -16 mgals in the southern section, 9 km south of the Clark Fork River. Figure 17 presents an analysis of the derivative maxima in horizontal direction from the method of Blakely and Simpson (1986). Gradient maxima analysis is a excellent first order method of locating faults (Reynolds, 1997). The steepest gradient of approximately -7.4 mgals/km is on the northern edge of the basin. The eastern and western sides of the basin have a gradient of approximately -5.5 mgals/km and –3.0 mgals/km, respectively. The southern gradient is approximately –3.3 mgals/km. The edges of the anomaly on the east and west are approximately 10 km in length. The northern and southern boundaries are approximately 6 km in length. The gradients are a good first estimate of the boundaries of the deep basin bounding structure, in this case large normal faults on the south, east and west, and the Lewis and Clark fault system on the north.

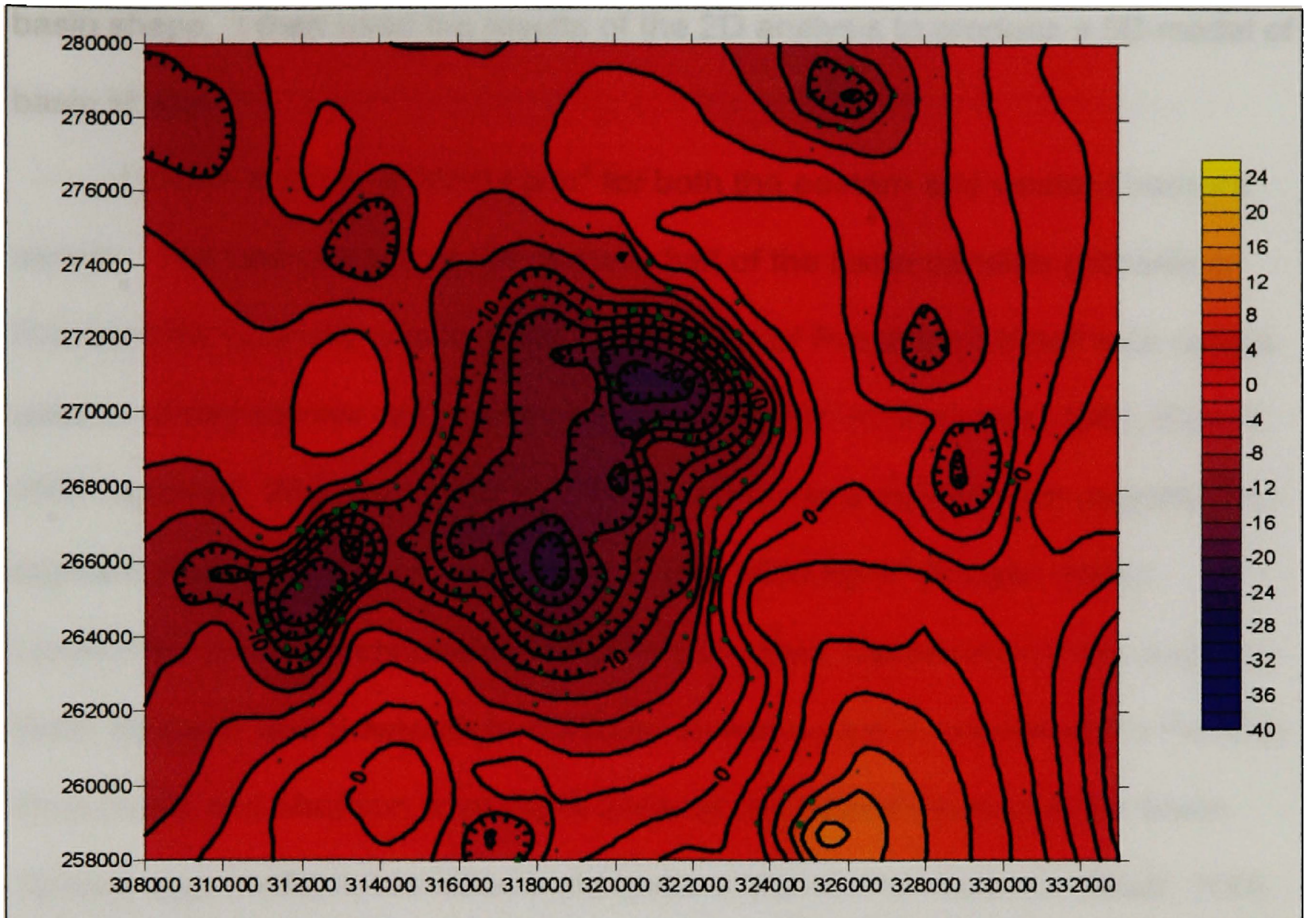

Figure 17. Gradient analysis of residual gravity data. The size of the green dots represents the size of the gradient. Larger green dots represent possible faults. There is strong correlation to the Lewis and Clark line in the north of the basin. The placement of the fault described in this study lies in the zone of larger green dots on the eastern portion of the basin

2D and 3D depth models

Density

The main purpose of my research is to estimate depth to bedrock beyond the areas where seismic or well data is available. To do this, I used 2D gravity modeling to first estimate density contrasts within the basin, then to identify a family of reasonable models, and finally to learn the general characteristics of the basin shape. I then used the results of the 2D analysis to produce a 3D model of basin shape.

I chose a value of 2800 kg/m^3 for both the eastern and western bedrock density. The bedrock under the western half of the basin consists primarily of Precambrian quartzite and argillite. The density of Precambrian Belt rock ranges used in similar studies range from 2600-2900 kg/m^3 (Constenius, 1987, Evans, 1997, Nyquest, 2001), which is similar to the standard densities for quartzite and argillites elsewhere, which range from 2700 - 3000 kg/m^3 (Burger, 1992). Limestone, shale, sandstone of the Colorado group, sandstones of the Jurassic Swift, Reirdon, and Sawtooth formations, as well as the limestone of the Permian Phosphoria and Madison formations underlie the eastern portion of the basin. Tertiary aged mafic dykes intrude the rocks of the eastern bedrock (Bhatt, 1964, Rasmussen, 1968, Lewis, 1998, Portner, 2004, Kunz, 2003, Fields et al., 1985) and raise the average density of these rocks.

Burger (1992) and Reynolds (1997) report that limestone densities range from 2500-2800 kg/m^3, shale ranges from 2000-2700 kg/m^3, sandstone ranges from 2000-2600 kg/m^3, and basaltic rocks range from 2700-3100 kg/m^3. The predominance of limestone in the eastern bedrock stratigraphy as well as intrusions of mafic rocks lead me to use the higher values on the ranges for the eastern bedrock making them equivalent to density values for the Precambrian quartzite. Thus, there will not be a gravity anomaly from juxtapositions of these rocks beneath the basin fill. My assumption of a homogenous bedrock density value for both the Precambrian Belt bedrock, and Cretaceous limestone bedrock, makes for somewhat easier gravity modeling but should be remembered when considering accuracy versus precision of the models as should the ranges of densities, thus the final density contrasts.

The Tertiary basin fill consists of unconsolidated to consolidated silts, sand, and isolated conglomerates with layers of volcanic ash. Density for similar sediments ranged from 800-2500 kg/m^3 (Constenius, 1989, Wells 1984, Evans 1997) and may vary with depth due to composition, diagenesis, compaction and saturation. I chose to model the basin fill as one uniform density average, averaging loose unconsolidated sediments at the top (500-800 kg/m^3) and more compact layers at depth (2000-2500 kg/m^3).

I chose the final density value of 1900 kg/m^3 for the basin fill by a forward modeling best-fit solution (Fig 18). I compared the mean difference between the observed bedrock depths provided by wells and my seismic lines, and depth values calculated by 2D (Table 2). I made iterative changes in bedrock/basin fill density contrasts to find the closest fit with observed bedrock depths. The final density estimation of 1900 kg/m^3 is low compared to the Bitterroot valley sediments (2000-2300 kg/m^3), and the Deerlodge sediments (2400-2700 kg/m^3) (Wells, 1986, Constenius, 1987). I believe the abundance of conglomerate in the Tertiary of the Bitterroot valleys and the abundance of carbonate clasts in the Deerlodge basin compared to the silt and mud abundant in the Tertiary of the Flint Creek basin could account for the density difference.

Station Information				Depth calculations for given density contrasts in kg/m^3											
point #	Type	Gbs	Obs z	1500	obs-calc	1000	obs-calc	900	obs-calc	800	obs-calc	650	obs-calc	500	obs-calc
9-28-1 a	Seis	-1.0	24.6	16.2	8.4	26.8	2.2	**26.8**	**2.2**	30.2	5.6	31.9	7.3	49.8	25.2
9-28-1 c	Seis	-1.2	30.6	21.5	9.1	37.0	6.5	**32.9**	**2.4**	44.3	13.8	55.2	24.7	52.3	21.8
9-28-1 b	Seis	-2.0	45.6	16.1	29.5	50.6	5.0	**56.0**	**10.4**	63.2	17.6	78.2	32.6	103.5	57.9
9-28-2 a	Seis	-2.0	65.6	16.1	49.5	50.6	15.0	**56.0**	**9.6**	63.2	2.4	98.2	32.6	130.3	64.7
9-28-2 b	Seis	-2.0	67.0	16.1	50.9	50.6	16.4	**56.0**	**11.0**	63.2	3.8	78.2	11.2	103.5	36.5
9-28-2 c	Seis	-1.5	32.3	23.3	9.0	38.2	5.9	**35.4**	**3.1**	46.7	14.4	58.5	26.2	76.6	44.3
9-21-1 a	Seis	-1.0	44.8	16.2	28.6	26.8	18.0	**26.8**	**18.0**	30.2	14.6	31.9	12.9	49.8	5.0
9-21-1 b	Seis	-1.5	49.9	23.3	26.6	38.3	11.6	**35.4**	**14.5**	46.7	3.2	58.5	8.6	76.6	26.7
9-21-1 c	Seis	-2.0	49.0	32.2	16.8	50.6	1.6	**56.0**	**7.0**	63.2	14.2	78.2	29.2	103.5	54.5
9-21-2 a	Seis	-2.0	43.7	32.2	11.5	50.6	6.9	**56.0**	**12.3**	63.2	19.5	78.2	34.5	103.5	59.8
9-21-2 b	Seis	-2.5	77.6	41.4	36.2	62.1	15.5	**69.6**	**8.0**	77.3	0.3	98.2	20.6	130.3	52.7
9-21-2 c	Seis	-2.0	52.6	32.2	20.4	50.6	2.0	**56.0**	**3.4**	63.2	10.6	78.2	25.6	46.0	6.6
Wilson 1	Well	-15.0	502.0	273.6	228	432.2	69.8	**487.0**	**15.0**	561.6	59.6	719.4	217.4	987.4	485.4
Wilson 2	Well	-10.0	298.2	176.2	122	245.2	53.0	**309.7**	**11.5**	353.6	55.4	445.5	147.3	604.5	306.3
	Density in kg/m^3			1500		1000		900		800		650		500	
	Mean diff Obs z - calc z (m)			46.20		16.39		**9.17**		16.79		45.05		89.10	

Table 3. Observed vs. calculated depths from 2D modeling at various density contrasts between bedrock (2800kg/m^3) and basin fill (1300-2300 kg/m^3).

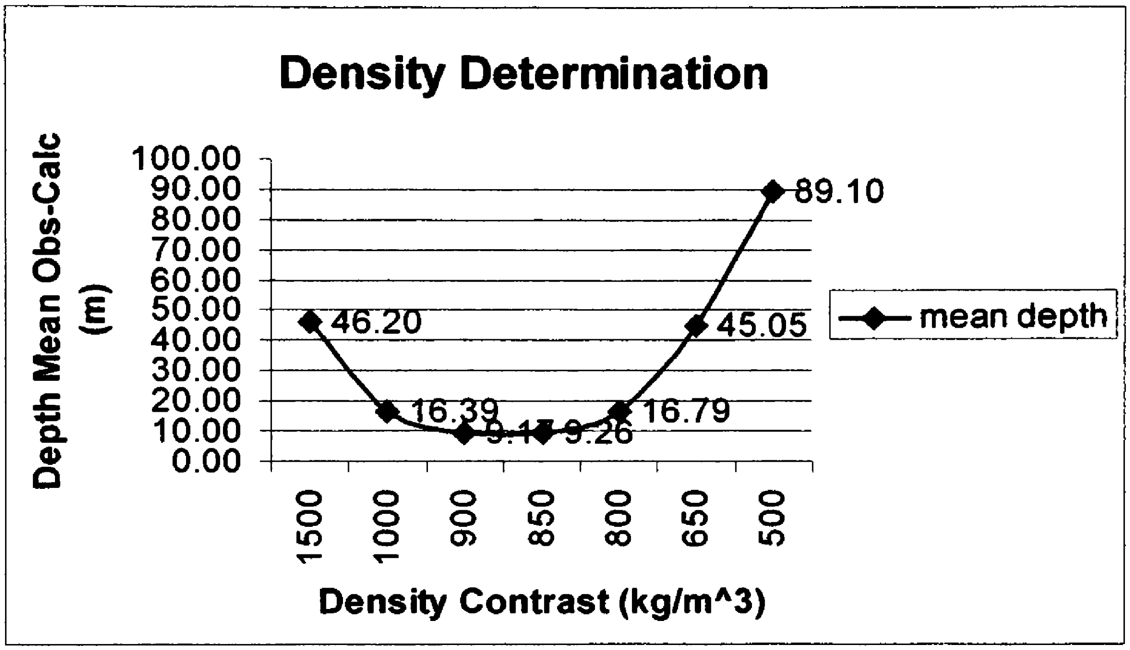

Figure 18. Density contrast verses mean depth difference. The lower the difference between observed depth and depth calculated by the 2D sections the more accurately the model is depicting the basin, thus areas without the benefit of depth data. I chose a final density difference of 900 kg/m^3 for the basin based on the 2D model data.

Inverting gravity data for depth estimates benefits greatly from having some constraints such as known bedrock depths. In this study I was fortunate enough to have two wells drilled to bedrock (Fig 2), my six seismic surveys, and the mapped bedrock contacts. I used the wells, seismic lines, and bedrock to constrain my 2D models (Table 2). Using the seismic data for constraints in the 2D models did not compromise the basic assumption that values of gravity at any point on the cross section are equal with any point perpendicular to the cross sections, because they are acute observations of relatively thin Tertiary sequences and should not be affected substantially by lateral changes in gravity. In contrast I relied heavily on the well data and bedrock contacts to test my 3D model accuracy. My 3D model is calculated using gravity changes in all directions from a point, so lateral fluctuations in gravity can cause calculated depths to have an erroneously high error when compared with the seismic observations. In the 3D model the depth of the wells let me model the whole package of Tertiary sediments and quantify the entire basin fill as one unit.

The wells used were Trans Texas Oil Company's Wilson 2 (well id 25039210090000) and Wilson 1 (well id 25039210080000) (Appendix 4, Fig 2). Wilson 2 is drilled 298 m through lacustrine beds into coarse quartzite gravel with a grain composition similar to Precambrian quartzite found in the area. I am assuming this gravel represents the first pulse of high-energy sediment activity following normal faulting in the basin and thus is close to the base of the Tertiary sediments and close to the bedrock surface. Wilson 1 is drilled to a depth of 990m through 502m of siltstone, mudstone and limestone until reaching clean hard sandstones. I am assuming the upper 500m, which resembles descriptions of the Renova outcrop sediments, represent the Tertiary sequence and the clean hard sandstones are the Precambrian bedrock. This depth is subject to interpretation, but I am assuming the change from sub-lacustrine/marine sediments to clean mature sandstones represents the fill/bedrock interface. I am using the fact that no Cretaceous rocks outcrop at the surface of the western side of the basin to rule out any subsurface Cretaceous layers in this well. The two wells provided control points of 298m and 502 m respectively for both the 2D, and 3D models. The Seismic lines described earlier provide depth to bedrock on the eastern portion of the basin, and the bedrock contact provided edges for all models. Because I know the gravity and depth at these wells, contacts, and seismic lines, I can use them and the density estimates along with all the remaining gravity observations to calculate basin depth where they are currently unknown.

2D

I used GRAVCADW (Sheriff, 1997) a 2D forward modeling program based on the Talwani (1959) algorithm to make my 2D gravity models. I then used my calculated best fit density contrast to construct three 2D cross sections (Fig 2) two perpendicular, and one parallel to the basins strike (Figs, 19-21).

Cross-section A - A' (Fig 19) crosses 5km west to east over the northern gravity depression. The gravity profile drops dramatically down from the bedrock gravity contact (0 mgals) on the eastern side reaches the maximum low (-21 mgals), then slopes upward to the western terminus. The dip then changes to a shallow 20° dip west reaching the maximum depth of 730m, 8 km from the eastern bedrock exposure. This cross section seems to show a steep normal fault on the eastern boundary.

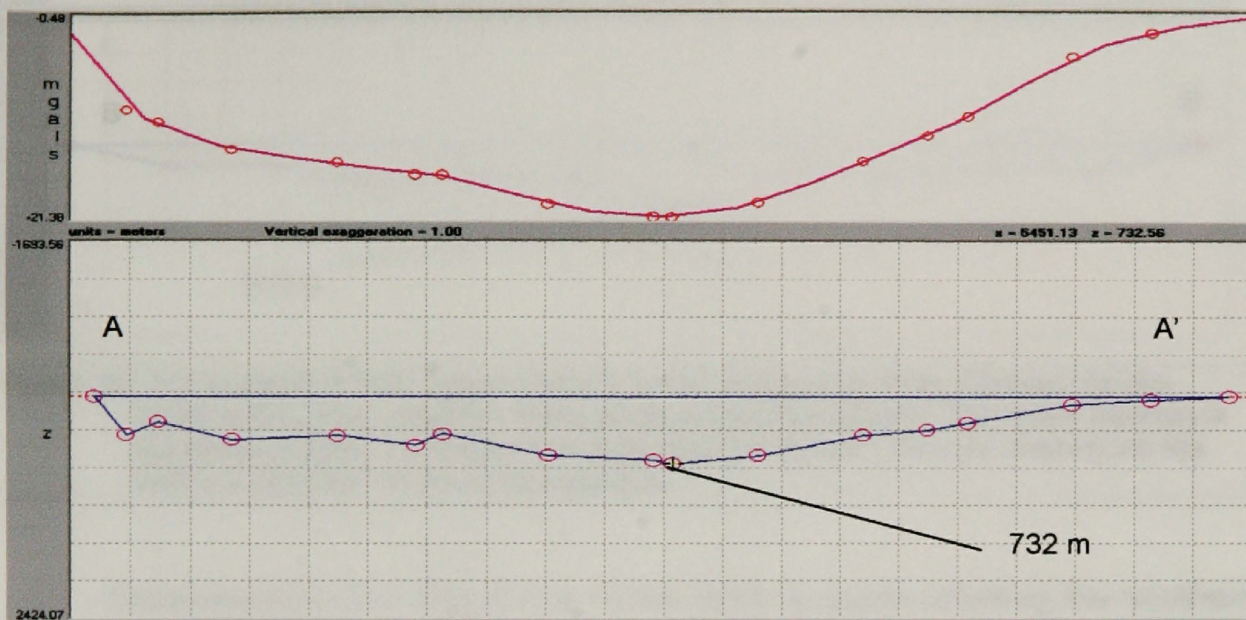

Figure 19. Cross section A-A'. Upper section is the modeled gravity anomaly for the basin in the lower section. Red points are known gravity. The lower section is the basin profile. The black line indicates the lowest point (in meters) on the bedrock surface for the cross section.

Cross-section B-B' (Fig 20) is located across the southern gravity low. The gravity signature is symmetric from east to west, and reaches a maximum gravity low almost in the center of the cross section. The bedrock topography is similarly symmetric with shallow 20°- 30° dips on the distal ends suddenly dropping off a scarp 450 m at symmetric 40°dip angles in the center of the basin. This cross section has a lack of gravity stations on the eastern flank; consequently the shape of the eastern fault is subdued and dissimilar to the northern cross section. I believe with better gravity data in this area would revel a similar fault as the line A-A'.

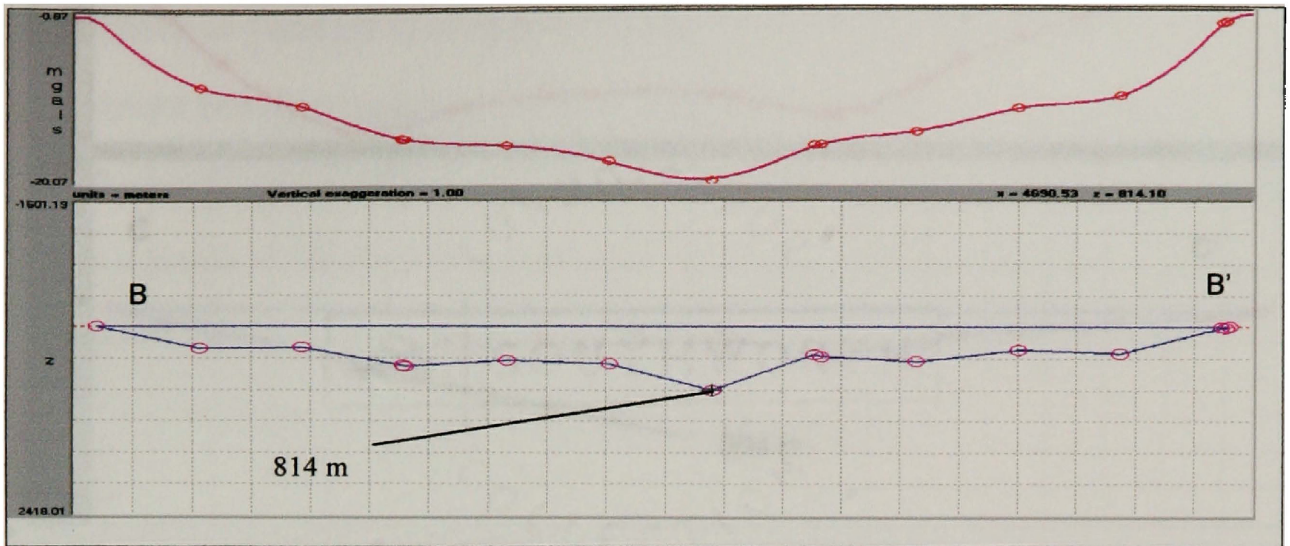

Figure 20. Cross section B-B' Upper section is the modeled gravity anomaly for the basin in the lower section. Red points are known gravity. The lower section is the basin profile. The black line indicates the lowest point (in meters) on the bedrock surface for the cross section.

Cross-section C-C' (Fig 21) is 15 km north to south crossing the southern and northern gravity anomaly parallel to the strike of the basin. The bedrock appears to gently dip south at 20° -30° to a maximum depth of 900 m, 2.5 km from the northern boundary. The southern portion dips north at 30° to the maximum depth point. There is also a low amplitude bedrock high in the center of this cross section, which is probably related to the downthrow on the northern and southern faults or smaller antithetic faults perpendicular to the strike of the basin.

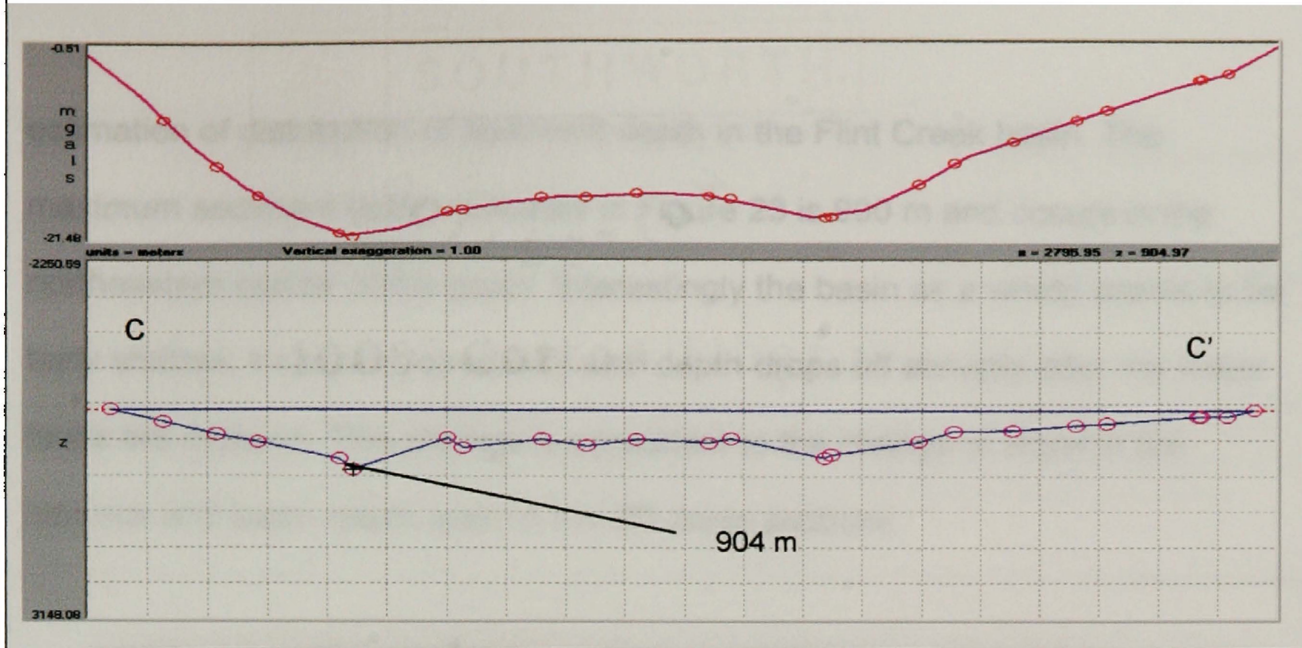

Figure 21. Cross section C-C'. Upper section is the modeled gravity anomaly for the basin in the lower section. Red points are known gravity. The lower section is the basin profile. The black line indicates the lowest point (in meters) on the bedrock surface for the cross section.

3D Model

My 3D depth models were created using GI3, an iterative gravity inversion method developed by Cordell and Henderson (1968). The input to the program is the residual anomaly gridded at an interval of 50 X 50 data points. This program also requires all values to be negative. I re-gridded the residual map (Fig 10) and used density contrasts of -900 kg/m^3 and –700 kg/m^3 to model sediment depth with gravity signature. I contoured the basin depth results using SURFER (Fig 22) and compared the depths calculated by GI3 to the known points of depth from the bedrock wells.

My 3D model results are similar to my 2D results. I used the 2D density contrast analysis to constrain the modeled density in the 3D models and compared density contrasts of –700, and -900kg/m^3 (Table 4)(Fig 22). The -900 kg/m^3 model has a better fit to the observed data and is presented as my final estimation of distribution of sediment depth in the Flint Creek basin. The maximum sediment depth indicated in Figure 23 is 900 m and occurs in the northeastern corner of the basin. Interestingly the basin as a whole seems to be fairly shallow, increasing gradually until depth drops off abruptly after the major faults are crossed. This change is consistent to the change of slope in the bedrock and basin depth seen in the 2D cross sections.

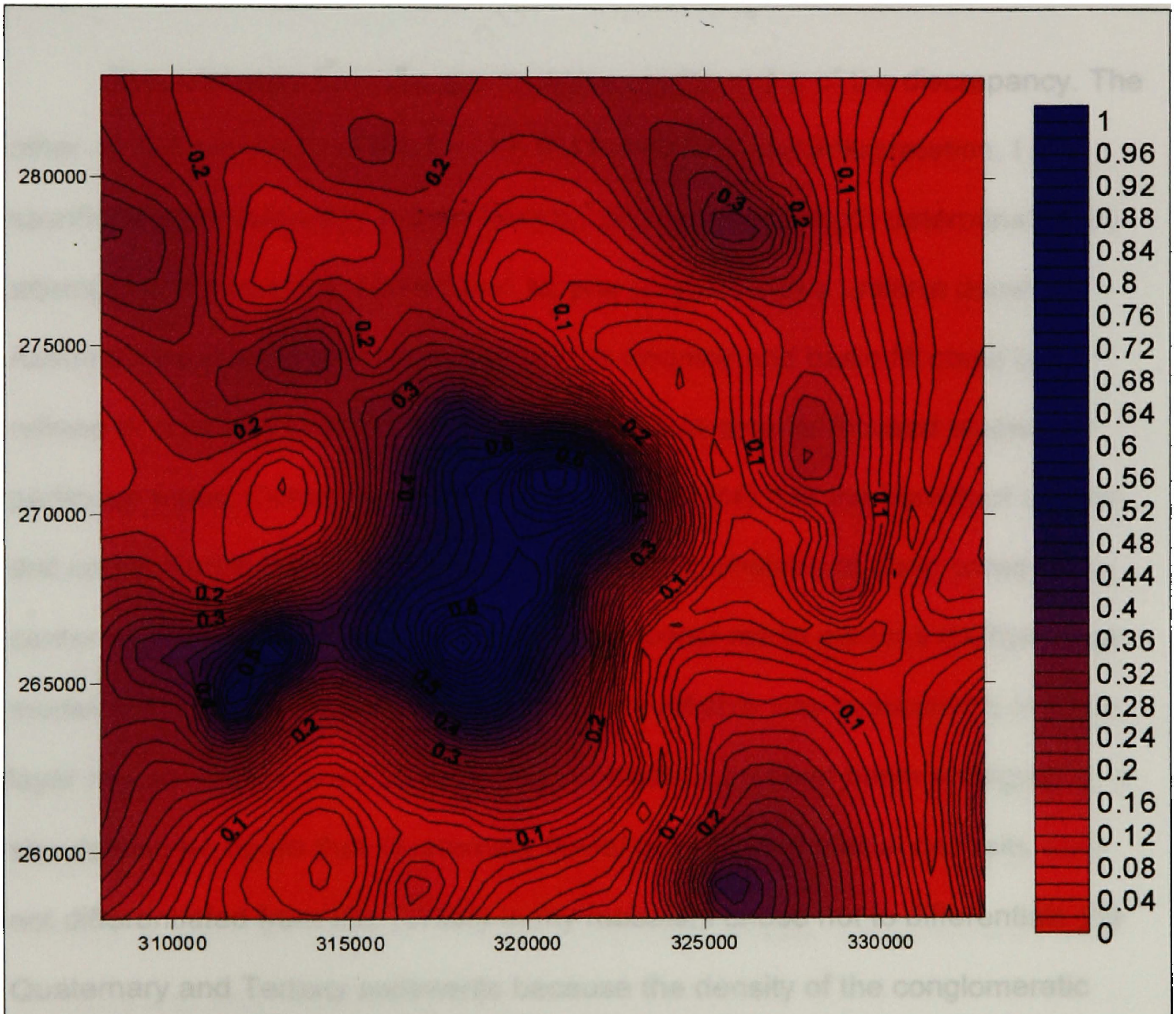

Figure 22. 3D basin model. Color scale is sediment depth in km. The deepest sediment depth is roughly 800m in both the northern and southern portions of the basin

Bedrock well	obs grav	Obs z	-700 kg/m^3	obs-calc	SQRTobs-calc^2	-900 kg/m^3	obs-calc	SQRTobs-calc^2
							0	0
Wilson 1	-18.5	502	448	54	54	498	4	4
wilson 2	-15.0	298.17	301.55	-3.38	3.38	320	-21.83	21.83
		Mean diff (m)			28.69			12.92

Table 4. Comparison of observed bedrock depth from wells and calculated bedrock depth from the 3D gravity model. The mean difference of using a density contrast of 900 kg/m^3 yields a more accurate depth estimation compared to observed depths.

The total error from the gravity accounts for +/-5m of the discrepancy. The other +/- 5m are errors related to drill log inaccuracy and interpretation. I also sacrificed some accuracy in both density, and sediment depth determination by attempting to model the entire basin as one polygon with a uniform density. Assumptions related to homogeneity of the bedrock and basin fill could be refined or changed to heterogeneous models with smaller focused studies on particular areas. Constenius (1989) and Wells (1984) had the benefit of several drill cores. Sediment description and stratigraphic analysis of deep cores in the center of the Flint Creek basin would have allowed me to model a multiple layer model accurately. I did not feel there was any reliable way to support a multiple layer model without more constraining information on deep basin stratigraphy. It should also be noted that Quaternary fluvial gravels, and glacial deposits were not differentiated from the Tertiary in my models. I chose not to differentiate the Quaternary and Tertiary sediments because the density of the conglomeratic fluvial deposits and glacial alluvial deposits are identical to unconsolidated Tertiary sediments and thus indiscernible with the geophysical methods presented.

Discussion

This study successfully refines the present understanding of the depth and distribution of sediment depth as well as the location of basin bounding faults in the Flint Creek basin. My study additionally provides valuable data for the congruent mapping project as well as basin evolution theories and models of the northern Rocky extensional region.

Faulting

The Lewis and Clark fault system truncates the Flint Creek Basin on the North, and a large mapped normal fault bounds it in the south. Both of these features are visible as steep gradients on the residual map (Fig 16) A large unmapped normal fault bounding the east of the basin is shown by gradient analysis of the residual anomaly (Fig 17). This unmapped fault is alluded to in Rasmussen's sedimentary analysis of the Flint Creek area as a probable source of subsidence for the deposition of the Renova Cabbage Patch formation. I drew probable locations of all faults on the residual map using the gradient analysis, my 2D models and mapped surface geology (Fig 23). Mapped normal faults in the Cretaceous bedrock can be extrapolated into the Tertiary connecting with my probable faults. My drawn faults are not visible in the surface geology in the Tertiary, suggesting that the fault may have been eroded, and covered by Mid - Miocene and later Tertiary gravels.

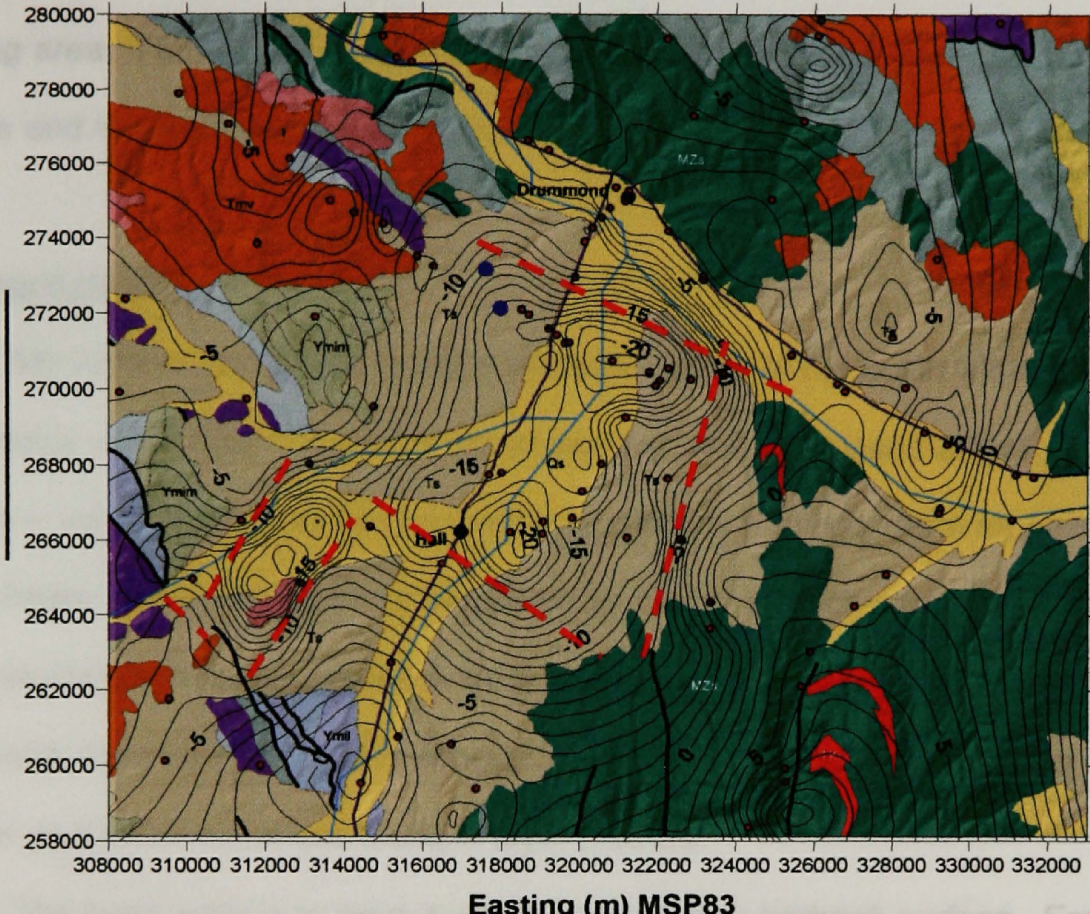

Figure 23. The red dashed lines are proposed faults buried below younger tertiary cover and are based on gravity gradient and seismic cross sections. Black solid lines are faults exposed in the bedrock

The fault on the east is somewhat discontinuous; this may be due to the normal fault being broken into different splays, being imbricate or discontinuous in nature. I interpret the lesser gradient on the western portion of the basin as a minor sympathetic normal fault or simply a bedrock fill contrast associated with down-throw on the eastern fault. The exact location of the fault splay on the southeastern margin is difficult to draw due to sparse data points and thus poor gravity gradient control on the southeastern edge of the basin. Exact mapping locations of these faults in my study should be viewed as a first estimation of the gradient analysis and an excellent starting point for more focused surveys in the faulting area. I am however confident in the placement of the faults on my figures and in the ongoing geologic mapping of the area.

Sediment depth

My 2D and 3D models provide sediment depth of the basin within a confidence of +/- 10m. There are some assumptions, discussed above, that are tied up in my analysis that can be used to qualify my findings. I am modeling the entire basin Tertiary/Quaternary sequence as one unit which can lead to error. I was fortunate to have two bedrock wells as well as my seismic lines for depth constraint, but more points of bedrock control would increase the accuracy of my models and allow me to use multiple layer models.

The basin seems to have a classic half-graben bedrock surface. Erosion of the original fault shoulders may have caused the change in dip seen in the 2D cross sections. The sediments seem to follow this model as well. The western portion displays relatively shallow depths that drop off dramatically at the inferred fault location into the deeper part of the basin. The eastern 3.5 km seem to gradually thin from the deep portion to the bedrock of the eastern basin margin. The fault contact, thus basin shape and depth, is not continuous from north to south and is reflected in the basin's overall residual signature (Fig 16).

Conclusions

I believe the large eastern fault, and as a consequence the Flint Creek basin, was formed by regional extension creating a graben structure that is reflected by the large box-like gravity low seen in the residual gravity signature (Fig 16). Furthermore I believe the increase in depth to the north of the basin seen in both the 2D and 3D models is due to transform movement on the Lewis and Clark fault system simultaneous with normal movement on the eastern normal fault creating a trapdoor basin. The transform movement increases the magnitude, and perhaps rate, of the normal fault movement.

Other examples of a pull apart or trapdoor basin are described in the Sierra Nevada ranges of California (Healy, 1964) and more generally in reference literature (Allen et al., 1990, Evans 1997). Evans (1997) described an analogous local example in the north east of the Missoula valley. The northeastern portion of the Missoula valley is interpreted as a trapdoor basin with a lateral component of movement provided by the Ninemile fault, and vertical movement on the Mt. Sentinel fault (Evans, 1997). This creates an abnormally deep area where the two faults meet. The left lateral movement on the Lewis and Clark line would "pull" the normal fault down faster on the northern edge of the eastern fault increasing the accommodation space and sediment depth to the north of the basin.

The flanking Deerlodge basin provides further evidence for extensional basin formation in the Flint Creek basin. The Deerlodge basin is interpreted by McLeod (1987) as a detachment structure with a large normal fault bounding its western edge, and a smaller antithetic fault bounding its eastern edge. I believe this is similar to the arrangement, but opposite in orientation, in the Flint Creek basin. The large basin bounding fault is in the east and a minor antithetic fault is in the west. Rasmussen (1979) described genetic similarities in the Late Eocene Cabbage patch formation (upper Renova) that crops out in the Upper Deerlodge Valley, and the Flint Creek basin suggesting the two shared a depositional low. I believe the proximity of the two basins geographically, their similar shape, stratigraphic similarities, and similar physical truncation by the Lewis and Clark system support a similar creation and evolution between the Flint Creek and Deerlodge basins. This allows me to use structural and stratigraphic relationships described in the Deerlodge basin as a direct comparison to those in the Flint Creek basin.

Future Studies

This study provides a better understanding of the general basin fill distribution in the Flint Creek basin where sediments are deepest and indicates the presence of a series of large normal faults located on the eastern edge of the fault that correlate to faults in the Cretaceous bedrock to the south.

Helpful topics for future studies would be seismic reflection or refraction studies in the deep portions of the basin to help constrain the edges of the faults and refine estimates of depth to bedrock. Drill core recovery and core analysis of the deeper Tertiary sediments in the basin would help constrain density contrasts by qualifying and quantifying the stratigraphic relationships and distribution. This data would be helpful to further refine a gravity model and produce a multilayer Tertiary density model. Additional mapping of the surface Tertiary units would help decipher the structure and timing involved in the normal faulting, as well as the relationship with depositional environments. Groundwater studies such as an isotopic tracer experiment as well as geochemical residence time studies would give insight into regional groundwater flow and the source of recharge to the groundwater in the Flint Creek basin.

References

Axelrod, Russel B. (1982) Tertiary Sedimentary Facies, Depositional Environments, and Structure, Jefferson Basin, Southwest Montana. *M.S. thesis, University of Montana, Missoula*, MT

Bhatt, B.K. (1967). Petrology and Stratigraphy of the Swift and Morrison Formations near Drummond Montana, USA. *M.S. Thesis. University of Montana*, Missoula, MT.

Burger, Robert, H. (1994) Exploration Geophysics of the Shallow Subsurface. *Prentice Hall*, Englewood Cliffs, NJ.

Constenius, Kurt. (1987) Structural Configuration of the Kishenehn Basin Deliniated by Geophysical Methods, Northwestern Montana and Southeastern British Columbia. *The Mountain Geologist*. Vol 25, No 1, p 13-28.

Evans, Catherine (1997) A Constrained Gravity Model of the Central Missoula Valley and Shape of the Ninemile Fault. M.S. Thesis, University of Montana, Missoula MT.

Robert W. Fields, Donald L. Rasmussen, Alan R. Tabrum, Ralph Nichols. (1985) Cenozoic rocks or the Intermontane Basins of Western Montana and Eastern Idaho: A Summary. *Rocky Mountain Section S.E.P.M. Cenozoic Paleogeography of the West Central United States. R.M. Flores and S.S. Kaplan, Editors*. Denver Colorado.

Gwinn, V. E. (1960) Cretaceous and Tertiary Stratigraphy and Structural geology of the Drummond area, Western Montana. *Unpublished Ph.D. Thesis*, Princeton University

(1961) Geology of the Drummond area, Central Western Montana. Mont. Bur. Of Mines and Geology. Specl. Pub. No. 21, Geol map No. 4

Hall, D.H., Hajnal, Z. (1962). The Gravimeter in Studies of Buried Valleys. *Geophysics*, Vol XXVII, No 6, part II, pp 939-951

Hanneman, D.L., Wideman, C.J. (1991) Sequence Stratigrapy of Cenozoic Continental rocks, Southwestern Montana. *Geological Society of America Bulletin*. Vol. 103, p 1335-1345.

Healy, J.H., Press, Frank. (1964). Geophysical studies of Basin Structures Along the Eastern Front of the Sierra Nevada, California. *Geophysics*. Vol. XXIX, p 337-359

Ibrahim, Abdelwahid, Hinze, William J. (1972) Mapping Buried Bedrock Topography with Gravity. *Groundwater,* Vol. 10, No. 3, pp18-23

Janecke, S.U. (1994) Sedimentation and paleogeography of the Eocene to Oligocene rift zone, Idaho and Montana. *Geological Society of America Bulletin*, Vol. 106, p. 221-228

Janecke, S.U. (1995) Eocene to Oligocene Half grabens of East Central Idaho. *Northwest Geology*, Vol. 24 p. 159-199

Rebecca Kunz, (2003), The Alkalic Intrusions of Garrison, Montana: A Possible Extension of the Central Montana Alkalic Province. *M.S. Thesis, University of Montana*, Missoula, MT.

Last, B.J. and Kubik K. (1983). Compact Gravity Inversion. *Geophysics*, Vol. 48, No. 6, pp 713-721

Lowrie, William. (1997). Fundamentals of Geophysics. *Cambridge University Press*. Cambridge. U.K.

Matoush, Joseph, P. (2002). The Stratigraphic, Sedimentologic, and Paleogeographic Evolution of the Eocene-Oligocene Grasshopper Extensional Basin, Southwest Montana. *M.S. Thesis University of Montana*, Missoula, MT.

McLeod, P. (1987) Depositional Evolution of the Deerlodge Valley, Western Montana. *M.S. Thesis University of Montana*, Missoula, MT.

Nyquest, David (2001) A Bedrock Model Of The Hellgate Canyon And Bandmann Flats Area, Montana Through Constrained Inversion Of Gravity Data. *M.S Thesis University of Montana*, Missoula, MT

Oldenburg, Douglas W. (1974) The Inversion and Interpretation of Gravity Anomalies. *Geophysics*, Vol. 39, No. 4, p. 526-536.

Pardee, J.T. (1950) Late Cenozoic Block Faulting in Western Montana: *Geological Society of America Bulletin*, Vol. 61, p. 359-406

Portner, Ryan (2004) Tertiary Sedimentation and Structure of the Flint Creek Basin. *Unpublished M.S. Thesis, University of Montana*.(In Progress)

Rasmussen, Donald, L. (1977) Geology and Mammalian Paleontology of the Oligocene-Miocene Cabbage patch Formation, Central-Western Montana. *Ph.D. University of Kansas*

(1969) Late Cenozoic Geology of the Cabbage Patch area, Granite and Powell Counties, Montana. *M.S. University of Montana*, Missoula Montana.

Renyolds, John, M. (1997). An Introduction to Applied and Environmental Geophysics. *John Wiley & Sons, New York.*

Rimrock Geophysics (1993). SIPWIN Seismic Refraction Analysis Software. *Rimrock Geophysics*, Lakewood, CO.

Ruppel, E.T. (1993). Cenozoic Tectonic Evolution of Southwest Montana and East-Central Idaho: *Montana Bureau of Mines and Geology*, Memoir, 65, 62 pgs

Sears, James W. (1995) Middle Miocene Rift system in S.W. Montana: Implications for Initial Outbreak of the Yellowstone Hotspot. *Northwest Geology*, Vol 25.

Sheriff, Steven (1997). GRAVCADW 2D Gravity Inversion Modeling Software. *University of Montana*, Missoula, MT

Talwani, M.J., Worzel, L., and Landisman, M. (1959) Rapid gravity computations for two dimensional bodies with Applications to the Mendocino Submarine Fracture Zone. *Jour. Geophysical Research*, Vol. 64, p. 49-59

Wells, Ken, (1989) Digital Filtering and Modeling of the Gravity Field of the Bitterroot Valley, western Montana. *M.S. Thesis University of Montana*, Missoula, MT

Westaway I.J. (1989) Northeast Basin and Range Province Active Tectonics. *Geology*, Vol. 17, p. 779-783

Appendix I: Seismic lines

Source: Bison I Elastic wave Generator
Spacing: 5m between phones
8-12 stacks per line.
24 geophones per line

Geophone	distance	time (ms)	Geophone	distance	time (ms)
1	100	5	1	100	60.0 ms
2	105	16.5	2	105	64
3	110	26	3	110	60
4	115	34.5	4	115	60
5	120	54.5	5	120	59.5
6	125	64.5	6	125	58
7	130	77.5	7	130	56.5
8	135	91	8	135	54.5
9	140	98.5	9	140	54
10	145	107	10	145	49
11	150	104	11	150	50.5
12	155	111	12	155	48
13	160	114.5	13	160	44.5
14	165	115.5	14	165	41.5
15	170	113	15	170	39.5
16	175	117.5	16	175	37.5
17	180	126.5	17	180	34.5
18	185	127.5	18	185	32
19	190	130	19	190	21.5
20	195	135.5	20	195	18
21	200	0	21	200	14
22	205	0	22	205	10
23	210	136	23	210	6
24	215	141	24	215	2.5
Line	**921-01**		**Line**	**921-1 reversed**	
SP	**80m**		**SP**	**235.00 m**	

Geophone	distance	time (ms)	Geophone	distance	time (ms)
1	100	49	1	102	190
2	105	59	2	107	184
3	110	68.5	3	112	179
4	115	76	4	117	178
5	120	85	5	122	174
6	125	96.5	6	127	174.5
7	130	106	7	132	170
8	135	112.5	8	137	169.5
9	140	122.5	9	142	165.5
10	145	132	10	147	160
11	150	139.5	11	152	153.5
12	155	142	12	157	147
13	160	147.5	13	162	139
14	165	154	14	167	129.5
15	170	157	15	172	121
16	175	158.5	16	177	113
17	180	162	17	182	105
18	185	164.5	18	187	95.5
19	190	166.5	19	192	87
20	195	171.5	20	197	80.5
21	200	173.5	21	202	71
22	205	175	22	207	57.5
23	210	180	23	212	46.5
24	215	181.5	24	217	38
Line	**928-01**		**Line**	**928-01 Reversed**	
SP	**80m**		**SP**	**234m**	

Geophone	distance	time (ms)	Geophone	distance	time (ms)
1	100	182	1	100	47
2	105	179	2	105	59
3	110	174.5	3	110	67.5
4	115	170.5	4	115	77.5
5	120	167	5	120	86
6	125	166.5	6	125	92.5
7	130	163	7	130	100.5
8	135	160	8	135	108.5
9	140	159	9	140	120.5
10	145	153	10	145	125
11	150	150.5	11	150	138
12	155	143.5	12	155	147
13	160	134.5	13	160	151
14	165	129.5	14	165	158
15	170	122.5	15	170	162.5
16	175	112.5	16	175	166.5
17	180	102.5	17	180	168
18	185	95	18	185	171.5
19	190	83.5	19	190	176.5
20	195	74	20	195	177
21	200	66	21	200	178.5
22	205	58	22	205	181.5
23	210	51	23	210	0
24	215	42.5	24	215	183.5
Line	**928-02**		**Line**	**928-02 Reversed**	
SP	**235m**		**SP**	**80m**	

Geophone	distance	time (ms)	Geophone	distance	time (ms)
1	100	121	1	100	35
2	105	117	2	105	40
3	110	114.5	3	110	43
4	115	111	4	115	47.5
5	120	110.5	5	120	52.5
6	125	107	6	125	57
7	130	101.5	7	130	60
8	135	98.5	8	135	63.5
9	140	95	9	140	68
10	145	91.5	10	145	71
11	150	88.5	11	150	74
12	155	86.5	12	155	79.5
13	160	83.5	13	160	84.5
14	165	80	14	165	88.5
15	170	75	15	170	90.5
16	175	72	16	175	97
17	180	69	17	180	100
18	185	66.5	18	185	104
19	190	64	19	190	106
20	195	61	20	195	108
21	200	58	21	200	109
22	205	55.5	22	205	113.5
23	210	53	23	210	119.5
24	215	50	24	215	121.5
Line	**1011-01**		**Line**	**1011-01 Reversed**	
SP	**245m**		**SP**	**70m**	

Geophone	distance	time (ms)	Geophone	distance	time (ms)
1	100	60	1	100	23.5
2	105	57.5	2	105	27.5
3	110	54.5	3	110	29
4	115	53.5	4	115	31
5	120	52	5	120	34
6	125	49	6	125	35.5
7	130	48	7	130	37.5
8	135	0	8	135	39.5
9	140	45	9	140	40
10	145	43	10	145	44
11	150	39.5	11	150	43.5
12	155	39	12	155	45
13	160	39	13	160	48
14	165	37	14	165	50
15	170	36.5	15	170	52
16	175	34	16	175	53
17	180	33	17	180	55.5
18	185	30.5	18	185	56
19	190	27	19	190	56.5
20	195	25.5	20	195	60
21	200	24.5	21	200	61.5
22	205	24	22	205	64.5
23	210	23	23	210	66.5
24	215	20.5	24	215	70
Line	**1011-02**		**Line**	**1011-02 Reversed**	
SP	**245m**		**SP**	**70m**	

Appendix II: GPS Station Data

Long	lat	Easting	Northing	MSL	station	Datafile	
-113.158	46.65986	320301	274319.67	1215.82851C		r022023a	BS
-113.246	46.66323	313609.9	275010.64	1402.44595C		r022021a	
-113.238	46.66059	314218.5	274688.19	1411.43826C		r022021b	
-113.216	46.65085	315825.7	273529.16	1294.47224C		r022021c	
-113.18	46.63925	318484.6	272112.9	1267.75053C		r022021d	
-113.171	46.63502	319175.8	271609.87	1243.93512C		r022022a	
-113.168	46.6337	319379.6	271452.94	1233.00177C		r022022b	
-113.164	46.63203	319695.3	271253.35	1232.15338C		r022022c	
-113.149	46.6282	320810.6	270774.7	1228.56939C		r022022d	
-113.158	46.65986	320301	274319.67	1215.828510C		r022023a	BS
-113.158	46.65985	320298.8	274318.43	1215.54181A		r111513a	BS
-113.18	46.58556	318196.5	266154.98	1272.01752A		r111514a	
-113.17	46.5856	319014.2	266120.97	1271.09913A		r111514b	
-113.157	46.58854	319029.4	266446.97	1274.18184A		r111514c	
-113.141	46.58563	321185.1	266023.33	1307.39885A		r111515a	
-113.124	46.58572	322537.5	265970.17	1351.17836A		r111515b	
-113.112	46.56444	323314.2	263567.68	1409.55747A		r111515c	
-113.158	46.65985	320298.4	274318.9	1215.75158A		r111516b	
-113.158	46.65985	320298.6	274318.88	1215.42999A		r111516a	BS
-113.158	46.65985	320298.4	274318.39	1215.30611B		r112212a	BS
-113.151	46.60315	320525.1	268001.67	1262.58742B		r112213a	
-113.157	46.5963	320030.7	267263.06	1261.63523B		r112213b	
-113.136	46.62573	321763	270455.65	1246.70034B		r112213c	
-113.13	46.62675	322249.2	270546.4	1281.8435B		r112214a	
-113.134	46.62252	321913.5	270092.2	1270.546B		r112214b	
-113.123	46.62449	322814.8	270269.53	1246.66967B		r112214c	
-113.112	46.62584	323660.5	270380.12	1222.9938B		r112215a	
-113.158	46.65984	320298.1	274318.14	1215.53949B		r112215b	BS
-113.158	46.65984	320298.1	274318.14	1215.53941D		r022819a	BS
-113.198	46.53538	316552.4	260651.75	1368.25183D		r022820b	
-113.151	46.48525	319934.5	254917.55	1605.51364D		r022820c	
-113.188	46.51973	317302.8	258875.12	1425.3535D		r022821a	
-113.215	46.58544	315556.6	266266.69	1301.85286D		r022821b	
-113.158	46.65985	320301.1	274319.32	1216.67527D		r022822a	BS
-113.158	46.65986	320301	274319.64	1215.02261E		r031317a	BS
-113.212	46.58538	315768.7	266249.36	1299.66742E		r031317b	
-113.239	46.58547	313739.4	266355.67	1326.22163E		r031318a	
-113.244	46.58545	313291.7	266375.13	1331.53924E		r031318b	
-113.249	46.57806	312891.1	265572.35	1340.72975E		r031318c	
-113.269	46.57106	311326.5	264869.01	1365.53996E		r031319a	
-113.284	46.57106	310161.6	264925.21	1382.52687E		r031319b	
-113.27	46.58091	311283.3	265966.23	1359.20678E		r031319c	
-113.249	46.57096	312854.3	264784.48	1348.26939E		031319d	
-113.158	46.65986	320301	274319.64	1216.021310E		031320a	BS
-113.158	46.65866	320301.01	274319.64	1216.051F		r031418a	BS
-113.158	46.65876	320301.01	274319.64	1215.975F		r031420a	BS

*all locations are in UTM lat/long NADS 83/ Montana State Plane
BS denotes base station measurement.

Appendix III : Gravity Data

	Easting	Northing	MSL	drift-corrected	grav-diff	obs-grav	theo-grav	FAC	FAA	BC	SBA
1C	320301	274319.7	1215.8290	5358.685	0	980362.2	980770.1	375.2047	-32.70787	145.2915	-177.999
5C	313609.9	275010.6	1402.446	5319.064	-35.52594	980326.7	980770.4	432.7948	-10.94802	167.5923	-178.540
6C	314218.5	274688.2	1411.438	5317.129	-37.46053	980324.7	980770.2	435.5698	-9.869205	168.6669	-178.536
4C	315825.7	273529.2	1294.472	5337.184	-17.40573	980344.8	980769.3	399.4741	-25.03043	154.6894	-179.720
3C	318484.6	272112.9	1267.751	5332.92	-21.67041	980340.5	980768.2	391.2278	-36.49265	151.4962	-187.989
2C	319175.8	271609.9	1243.935	5337.454	-17.1356	980345	980767.8	383.8784	-38.9248	148.6502	-187.575
7C	319379.6	271452.9	1233.002	5339.504	-15.08555	980347.1	980767.7	380.5043	-40.12904	147.3437	-187.473
8C	319695.3	271253.3	1232.153	5335.665	-18.92532	980343.3	980767.6	380.2425	-44.08045	147.2423	-191.323
9C	320810.6	270774.7	1228.569	5335.449	-19.1406	980343	980767.2	379.1365	-45.05508	146.814	-191.869
10C	320301	274319.7	1215.829	5354.595	0.004679	980362.2	980770.1	375.2047	-32.70319	145.2915	-177.995
1A	320298.8	274318.4	1215.542	5358.6850	0	980362.2	980770.1	375.0817	-32.83015	145.2439	-178.032
2A	318196.5	266155	1272.017	5299.065	-35.85469	980326.3	980763.4	392.5446	-44.50704	152.0061	-196.513
3A	319014.2	266121	1271.099	5301.858	2.788098	980329.1	980763.4	392.2612	-42.00589	151.8963	-193.898
4A	319029.4	266447	1274.182	5306.654	4.789202	980333.9	980763.6	393.2125	-36.53091	152.2647	-188.784
5A	321185.1	266023.3	1307.399	5306.206	-0.454141	980333.4	980763.4	403.4633	-26.47182	156.2342	-182.689
6A	322537.5	265970.2	1351.178	5296.653	-9.556902	980323.9	980763.4	416.9736	-22.52616	161.4658	-183.970
7A	323314.2	263567.7	1409.557	5289.524	-7.136074	980316.8	980761.5	434.9894	-9.72288	168.4421	-178.137
8A	320298.4	274318.9	1215.751	5334.952	45.42227	980362.2	980770.1	375.1809	-32.73317	145.2823	-177.981
9A	320298.6	274318.9	1215.43	5334.962	0.002239	980362.2	980770.1	375.0817	-32.83015	145.2439	-178.032
1B	320298.4	274318.4	1215.306	5358.6850	0	980362.2	980770.1	375.1154	-32.88872	145.257	-178.084
2B	320525.1	268001.7	1262.587	5309.722	-26.56773	980335.6	980765	389.6345	-39.7197	150.8792	-190.587
3B	320030.7	267263.1	1261.635	5310.493	0.762546	980336.4	980764.3	389.3406	-38.63196	150.7654	-189.378
4B	321763	270455.6	1246.7	5314.139	3.638926	980340	980767	384.7317	-42.26225	148.9807	-191.218
5B	322249.2	270546.4	1281.843	5307.857	-6.288074	980333.7	980767.1	395.5767	-37.79738	153.1802	-190.947
6B	321913.5	270092.2	1270.54	5309.154	1.291202	980335	980766.7	392.0886	-39.6125	151.8295	-191.405
7B	322814.8	270269.5	1246.67	5318.814	9.654479	980344.7	980766.9	384.7222	-37.50249	148.977	-186.438
8B	323660.5	270380.1	1222.993	5327.046	8.226196	980352.9	980767	377.4156	-36.70454	146.1477	-182.791
9B	320298.1	274318.1	1215.539	5336.249	9.189479	980362.1	980770.1	375.1154	-32.88872	145.257	-178.084
1D	320298.1	274318.1	1215.539	5358.6850	0	980291.6	980770.1	375.2012	-103.3367	145.2901	-178.002
3D	316552.4	260651.8	1368.252	5310.005	-46.13	980245.4	980758.8	422.2425	-91.17419	163.5061	-184.044
4D	319934.5	254917.6	1605.514	5252.591	-57.41914	980188	980754.3	495.4615	-70.84232	191.8589	-192.061
5D	317302.8	258875.1	1425.353	5292.273	39.6781	980227.7	980757.4	439.8639	-89.87857	170.3297	-189.560
6D	315556.6	266266.7	1301.853	5320.171	27.89086	980255.6	980763.4	401.7518	-106.0405	155.5714	-190.960
7D	320301.1	274319.3	1216.675	5356.127	35.95224	980291.5	980770.1	375.466	-103.1	145.3927	-177.839
1E	320301	274319.6	1215.023	5358.685	0	980291.6	980770.1	375.0794	-103.4527	145.243	-178.0757
2E	315768.7	266249.4	1299.667	5322.514	-36.17107	980255.4	980763.4	401.0773	-106.894	155.3103	-191.5771
3E	313739.4	266355.7	1326.222	5318.359	-4.160736	980251.2	980763.4	409.272	-102.8679	158.4835	-190.7069
4E	313291.7	266375.1	1331.539	5315.137	-3.237693	980248	980763.4	410.913	-104.4631	159.1189	-192.9347
5E	312891.1	265572.4	1340.73	5313.141	-2.001417	980246	980762.7	413.7492	-102.9602	160.2172	-192.5257
6E	311326.5	264869	1365.54	5311.198	-1.947454	980244	978032.7	421.4056	2632.769	163.182	-192.8573
7E	310161.6	264925.2	1382.527	5311.46	0.255031	980244.3	978032.7	426.6478	2638.266	165.212	-189.2884
8E	311283.3	265966.2	1359.207	5318.25	6.785031	980251.1	978032.7	419.4512	2637.855	162.4252	-186.8376
9E	312854.3	264784.5	1348.269	5315.533	-2.721933	980248.4	978032.7	416.0759	2631.758	161.1182	-192.1046
10E	320301	274319.6	1216.021	5358.657	43.12199	980291.5	978032.7	375.2626	2634.066	145.3139	-177.9623

	TC	CBA
1C	0.714266	-177.2851
5C	0.217099	-178.3232
6C	0.256253	-178.2798
4C	0.304116	-179.4157
3C	0.297251	-187.6916
2C	0.254616	-187.3204
7C	0.27553	-187.1972
8C	0.33934	-190.9834
9C	0.388013	-191.4811
10C	0.70265	-177.292
1A	0.704489	-177.3273
2A	0.155962	-196.3572
3A	0.171756	-193.7258
4A	0.19299	-188.5911
5A	0.155285	-182.5333
6A	0.162577	-183.8079
7A	0.190231	-177.9463
8A	0.703002	-177.278
9A	0.704489	-177.3273
1B	0.703961	-177.3804
2B	0.202332	-190.3842
3B	0.221074	-189.1566
4B	0.367493	-190.8505
5B	0.2724	-190.6742
6B	0.297515	-191.1079
7B	0.336159	-186.1014
8B	0.514753	-182.2767
9B	0.703961	-177.3804
1D	0.716594	-178.0018
3D	0.102331	-183.9413
4D	0.112499	-191.9481
5D	0.03153	-189.5287
6D	0.088506	-190.8717
7D	0.698722	-177.1398
1E	0.704505	-177.3712
2E	0.094306	-191.4828
3E	0.075073	-190.6318
4E	0.059886	-192.8748
5E	0.052459	-192.4733
6E	0.026536	-192.8308
7E	0.031759	-189.2567
8E	0.040008	-186.7976
9E	0.045326	-192.0592
10E	0.716594	-177.9623